FOUR-WAVE MIXING AND BOSE-EINSTEIN CONDENSATION IN NANO-ELECTRO-OPTOMECHANICS

By

Sohail Ahmed

Department of Electronics,

Quaid-i-Azam University, Islamabad, 45320, Pakistan

This dissertation is submitted for the degree of

Master of Philosophy

July 2019

” Don’t be satisfied with stories, how things have gone with others.

Unfold your own myth.”

-Rumi

Dedicated

to

My Family and Friends

Certificate

It is certified that the work presented in this dissertation is accomplished by Sohail Ahmed under the supervision of Dr. Farhan Saif at Quaid-i-Azam University, Islamabad, Pakistan..

Research Supervisor:

_____

Dr. Farhan Saif

Professor

Department of Electronics

Quaid-i-Azam University, Islamabad, Pakistan.

Submitted Through:

_____

Dr. Aqeel Abbas Syed

Chairman

Department of Electronics

Quaid-i-Azam University, Islamabad, Pakistan.

Acknowledgments

I grasp this graceful moment to express my gratitude to the Heavens for the blessings which led me to write a manuscript like this.

I would like to be beholden to my Supervisor Professor Dr. Farhan Saif who granted me an opportunity to work with him. I am really honoured to be his student. His guidance at each and every step helped me to accompalish my work. I would not be able to finish this manuscript without his valueable suggestions and efforts.I also want to thank Dr. Arshad Hussain who motivated me towards research. I appreciate my colleagues who lended their helping hands to solve the problems which I faced in my work.

I am indebted to my parents for their support and sacrifice in making everything possible in my life. I am thankful to all those friends and relatives who have guided and facilitated me to complete this thesis.

Sohail Ahmed

July 2019

Abstract

In this dissertation we theoretically study the dynamics of a Nano Electro Optomechanical system (NEOMS) in the presence of a strong pump field and a weak probe field.The system consists of a Fabry-Perot cavity which is composed of a fixed and partially transparent mirror at one end and a fully reflecting movable mirror MR1 at the other end. MR1 is coupled to the intra-cavity field through optomechanical coupling. An additional movable micro-resonator MR2 is provided to the cavity which is electrostatically coupled to MR1 via Coulomb interaction. Mechanical driving fields ε_1 and ε_2 are applied to selectively pump the mechanical resonators (MRs).

A non-linear effect, in the probe transmission field, known as Four-wave mixing, is investigated in the Nano-electro-optomechanical system (NEOMS). The nonlinearity which is caused by the radiation pressure force of the intra-cavity field, gives rise to Four-wave mixing (FWM) phenomenon, which is equivalent to the nonlinear Kerr effect in optical fibers that causes a nonlinear susceptibility in the medium. Here this nonlinear effect is called effective Kerr effect, which is caused by the radiation pressure force and is responsible for Four-wave mixing (FWM).

In the probe transmission field, Four-wave mixing (FWM) is reported by selectively driving the mechanical resonators MR_1 and MR_2, which provides extra control of FWM. The FWM is observed to show consistent modifications by changing the amplitudes and phases of the external driving fields. We show in our results that significant suppression and amplification can be achieved in the FWM peaks by controlling the phases of external driving fields.

We also report enhancement in the FWM phenomenon, in the presence of Bose-Einstein Condensate (BEC) trapped inside the cavity. We show that the FWM intensity is greatly suppressed and amplified in the presence of atomic medium

(BEC) in the optical cavity. The intensities of FWM peaks change coherently by varying the value of atom-field coupling. Moreover, we show that the medium mediated FWM signal is efficiently controlled by selective mechanical drivings of MRs.

Contents

List of Figures

Chapter 1

Introduction

Light, most commonly known as photons, has been a predominant topic of discussion since the birth of physics. Light bears both classical and quantum effects. The quantum effect of light is studied in Quantum optics, the physics which investigates phenomena involving light (photons) and their interaction with matter at submicroscopic level [1].

It is commonly believed that Quantum mechanics only deals with the microscopic systems and particles having very small dimensions, particularly photons, atoms, electrons and sub-atomic particles but the scope of quantum mechanics is so wide that it also covers the very dynamics of macroscopic systems and devices.

1.1 Radiation pressure force

In a book about comets, astronomer Johannes Kepler noted that the tail of a comet always points away from the sun. His explanation says that the light emitting from the sun pushes away the tail. This is apparently the first known conjecture about the phenomenon of radiation pressure. James Clark Maxwell came up with a quantitative analysis for radiation pressure force and later in 1901, it was detected in laboratory (by Nichols and Hull in Dartmouth). Since then, radiation

pressure force has been investigated and exploited in various contexts, for example in influencing the motion of cold atoms or subatomic particles. Since the light only provides fixed forces, so the back-action of the mechanical motion onto the electromagnetic field is absent in such settings. However, this kind of two-way interaction is present in an optomechanical system [2].

The geometry of optical cavity in an optomechanical system changes due to the mechanical motion of the end mirror. This is termed as optomechanical effect. The question, how large this effect would be, depends on the geometry of the cavity and amplitude of mechanical motion. When an intense pump field is injected to the cavity, the incoming laser intensity is resonantly enhanced. The optical finesse of the cavity which is in order of million, is multiplied to the incoming laser field which increases the radiation force by the same amount. At the very same time, small changes in the boundary of the cavity induce a shift in the optical resonant frequency which leads to a rapid decrease of light intensity, which in turn decreases the radiation force. In this way the resulting motion acts back on the light field and as a result it modifies the radiation pressure force. This is a genuine interaction between light and mechanical motion, which is at the heart of optomechanics.

The radiation pressure force is considerable when it is exerted on particles and systems having very small dimensions such as electron, micro-resonators and micro mirrors etc. Cavity Optomechanics deals with systems involving optical field interacting with mechanical resonators, thus producing very interesting non-linear quantum effects which are measured by using well developed methods of quantum optics [2,3]. These systems are extensively used in series of developments such as sensors and actuators in integrated circuits, and optical systems [4,5]. The amended and modified dynamics of the mechanical system can be studied by observing the optical field which interacts with it. The efficiency of these systems depends on how the thermal environment interacts with them.

1.2 Cavity fields

In a typical optomechanical system, the cavity is driven by a strong laser field. This strong field creates the radiation pressure force. The photons of this intense pump field continuously strike the mirror and export their momentum to it, which in turn excite the movable mirror at some resonance frequency (by the continuous action of radiation pressure force). The intense laser field is accompanied by a weak probe field, to investigate the dynamics and internal changes of the system.

1.3 Hybrid optomechanical system

The framework of cavity based optomechanical system with other systems like, two-level atoms [12,13], mechanical membranes [14,15] and Bose-Einstein condensate [16,17,18], is regarded as Hybrid quantum systems [19,20]. One of such hybrid systems is quantum electro-optomechanical system (QEMS) [22,23], in which the mechanical and electronic parametric quantities are of great significance. In such systems, electrostatic Coulomb interaction provides an extra degree of freedom, with which the resolved side-band regime [27,28] can be reached. When this kind of electro-mechanical system is combined with quantum optomechanical system, a new type of hybrid system is formed, which is commonly known as Nano Electro Optomechanical system (NEOMS).

Nano Electro Optomechanical systems (NEOMS) bear the potential for efficient low-noise Nano-transducers between microwave and optical signals, both in classical and quantum domains. Such systems provide nano-scale precision for mechanical motion of the micro-resonators. The mechanical vibrations of the movable mirrors (micro-resonators) has a significant effect on the output signal of the probe field.

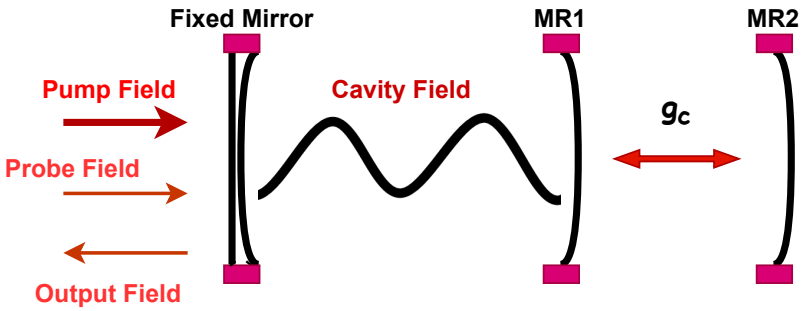

Figure 1.1: Schematic representation of the Nanoelectro-optomechanical system: MR_1 is coupled with the cavity field through optomechanical coupling g_0 and to the second mechanical resonator MR_2 through the coulomb coupling strength g_c.

This hybrid system couples optical, electrical and mechanical degrees of freedom. A typical Nano Electro Optomechanical system (NEOMS) is shown in Fig. 1.1. The system is composed of a fixed mirror and two movable mirrors (micro-resonators) MR1 and MR2. The cavity formed by the fixed mirror and movable mirror (MR1) contains the optical signal i.e, cavity field. MR1 is coupled to another mechanical resonator MR2 through electrostatic Coulomb interaction g_c. The advantage of these Nano electro Optomechanical systems (NEOMS) over quantum optomechanical systems is remarkable as these systems provide dynamic control of the flow of light in nanophotonic structures, at higher speeds and low power consumption.

1.4 Mechanical driving fields

The selective mechanical driving of mechanical resonators MR1 and MR2 provides an additional control of the probe transmission field in nano transducers. Symmetric and asymmetric amplifications and suppressions of the output signal can be achieved with selective acoustic control. Switchable signal amplification and light communications can be made possible by selectively driving the mechanical

resonators MR1 and MR2. For this purpose, mechanical driving fields with amplitude $\varepsilon_1(\varepsilon_2)$ at frequency $\omega_1(\omega_2)$, are shined on the mechanical resonators MR1 and MR2 respectively, as shown Fig. 1.2.

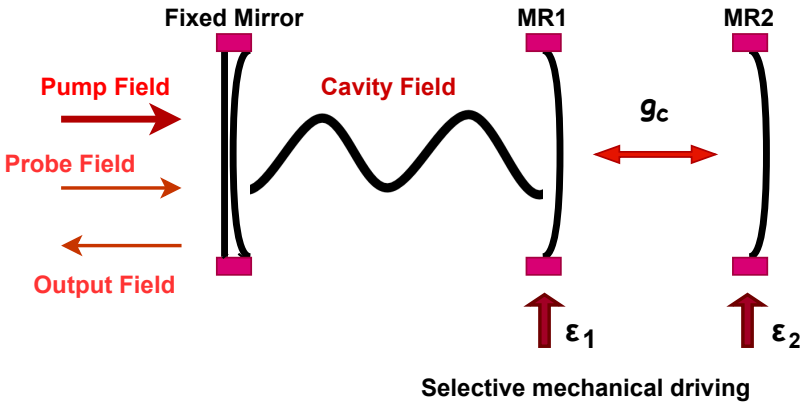

Figure 1.2: Schematic representation of the Nanoelectro-optomechanical system: MR_1 is coupled with the cavity field through optomechanical coupling g_0 and to the second mechanical resonator MR_2 through the coulomb coupling strength g_c. $MR_1(MR_2)$ is selectively driven by $\varepsilon_1(\varepsilon_2)$.

1.5 Non-linearities in Cavity based optomechanical systems (COMS)

As the input laser power increases, the relative fluctuations of the photon numbers become smaller. At some point, for higher laser powers an another effect kicks in, i.e the backaction of the vibrating end mirror onto the cavity field, which modifies the radiation pressure force. These unavoidable photon shot noise fluctuations of the laser beam exert a random force on the end mirrors which imprints some extra motion that masks the real signal. This is how non-linearities are introduced in the

cavity. One of these non-linearities is the effective Kerr effect [30,32], which arises from the radiation pressure force [18,19]. The concept of effective Kerr medium is due to the fact that the length of the optical cavity depends on the radiation pressure force. Because of the intensity dependent length of the cavity, the optomechanical coupling strength is changed. When the radiation pressure force is lowered, the mirrors displacement increases due to which the cavity length also increases and the whole story repeats itself. In this way the non-linearities come in the system that can be studied using well developed methods of quantum optics. Four-wave mixing (FWM) [45,46], electromagnetically induced transparency (EIT) [37,38,40], optomechanically induced transparency (OMIT) [17,18] and optical bistability [22,25] and multistability [41.42] are efficient tools to investigate the nonlinear nature of hybrid optomechanical systems.

1.6 Layout

In this dissertation, the dynamics of a cavity based hybrid Electro Optomechanical system is described in the presence of a strong pump laser. In addition to the intense pump field a weak probe field is injected into the cavity to scan the nonlinear optical features of the output light signal. In the **Second Chapter** we describe a basic cavity based optomechanical system (COMS) in which a cavity field is coupled to a moving end mirror through an optomechanical coupling.The intense pump laser and weak probe fields are injected into the cavity from the partially reflecting fixed mirror. The dynamics of the system is studied using the outgoing intracavity field. The abrupt changes in phase and amplitude of the outgoing cavity field tell about all the statistical information related to the dynamics of the system. An intermodulation phenomenon in non-linear quantum optics, known as Four-wave mixing, is theoretically studied using the probe transmission field of the system. Four-wave mixing (FWM) is a non-linear phenomenon

which arises due to the effective Kerr effect caused by radiation pressure force. In such a system, four-wave mixing is generated by the interference of reflected and transmitted light signal to the optomechanical coupling field. FWM is capable for understanding the nonlinear behavior of cavity based optomechanical systems (COMS). Four-wave mixing has promising applications in the quantum optical regime for generating single photons, squeezed light and entangled photons [6]. In this work, we investigate the behavior of four-wave mixing (FWM) intensity by driving the mechanical resonator MR1 externally. Switchable mechanical driving field ε_1 is applied to MR1, which provides an additional control of the FWM signal.

In the **Third Chapter**, we investigate the features of four-wave mixing light signal in a hybrid Electro optomechanical system commonly known as Nano Electro Optomechanical system (NEOMS).In this system a second moving-end mirror (MR2) is provided to the cavity, which is coupled to MR1 via electrostatic Coulomb interaction. The behavior of four-wave mixing (FWM) intensity is studied by selectively driving the two mechanical resonators MR1 and MR2. Switchable mechanical drivings of MRs provide a versatile route to realize switchable signal amplification in optical devices. In the **Fourth Chapter** of the thesis, we study the nonlinear FWM phenomenon in a Nano transducer (NEOMS), in the presence of Bose-Einstein condensate (BEC), trapped inside the Fabry-Perot cavity. In different areas of experimental physics, BEC plays very important role in studying and investigating the underlying mysteries. It has been found that Bose-Einstein condensate (BEC) is used as "Quantum Simulators" to stimulate condensed matter systems [7,8]. Researchers proposed that Bose-Einstein condensate (BEC) could be used to observe quantum mass acquisition [8]. A coherent optical non-linearity, known as Electromagnetically-induced transparency (EMIT) [9] and a useful measure of time distortion, known as Group delay [10], has been extensively studied using Bose-Einstein condensate (BEC) in different quantum

systems.

In this work, we report the enhancement of FWM intensity in the presence of atomic medium, i.e Bose-Einstein condensate (BEC), in the optical cavity. We show in our results that the medium mediated FWM signal is greatly suppressed and amplified by selectively driving the mechanical resonators MR1 and MR2.

Chapter 2

Controlled Four-wave mixing in an Optomechanical system

2.1 Objective of the work

In this chapter we shall cover the basic dynamics of an optomechanical system which is composed of a fixed and partially reflecting mirror at one end and a movable mirror at the other end. The optical cavity is coupled to the movable mirror (MR1) through an optomechanical coupling strength. Our work is based on the phenomenon of Four wave mixing (FWM) in which we report that FWM intensity is suppressed or amplified in the presence of switchable mechanical driving of the movable mirror MR1.

2.2 System Model

A basic Cavity optomechanical system (COMS) with a high finesse and single mode optical cavity is presented, as shown in Fig.2.1. The intracavity field exerts a radiation pressure force on the vibrating end mirror (MR_1) thus displacing it from its mean position, which in response modifies the radiation pressure force.

We consider a high Q Fabry-Perot cavity of length L, with a fixed mirror at one end and a movable mirror (mechanical resonator MR1) at the other end. Mechanical resonator MR1 is coupled to the cavity field through optomechanical coupling g_0.

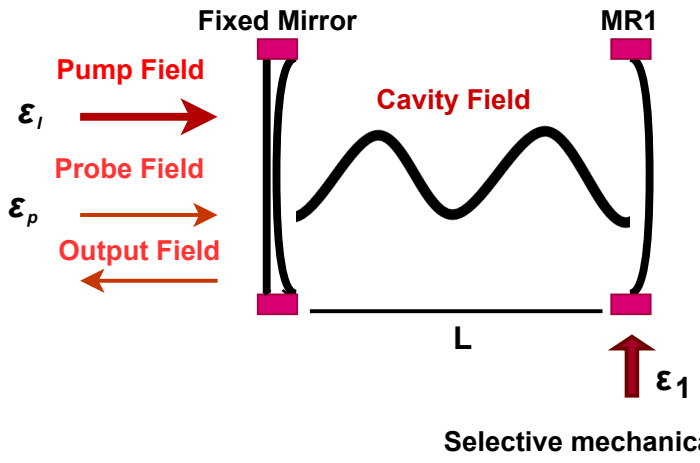

Figure 2.1: Schematic representation of a basic optomechanical system: MR_1 is coupled with the cavity field through optomechanical coupling g_0. A strong input laser field of amplitude ε_l and a weak probe field of amplitude ε_p are fed to the cavity through the fixed mirror. L is the length of cavity , ε_1 is the selective mechanical driving of MR_1.

A strong input laser field of amplitude ε_l and a weak probe field of amplitude ε_p are injected to the cavity through the fixed mirror. The radiation pressure force displaces the mechanical resonator MR1 from its mean position which changes the length of the cavity. To compensate this change the movable mirror exerts a backaction force onto the cavity field which lowers the radiation pressure and vice versa.

2.2.1 Total Hamiltonian of the System

We consider single mechanical mode for vibrating end mirrors, modeled as harmonic oscillator MR_1 with frequency ω_1, therefore the Hamiltonian of the mechanical resonator is given by

$$H_{MR_1} = \hbar\omega_1 {b_1}^\dagger b_1 \tag{2.1}$$

where ω_1 is frequency and ${b_1}^\dagger$ and b_1 are annihilation and creation operators of MR_1 with $[b_1, b_1^\dagger] = 1$.

The cavity is driven by a strong pump field $\varepsilon_l = \sqrt{\frac{2P_l\kappa}{\hbar\omega_l}}$ and a weak probe field $\varepsilon_p = \sqrt{\frac{2P_p\kappa}{\hbar\omega_p}}$ is injected into the cavity to scan the outgoing optical signal. Here κ is the cavity decay rate and P_l and P_p correspond to strong laser and weak probe field powers. We are interested in the free Hamiltonian for the cavity with frequency ω_c and photon creation(annihilation) operators $c^\dagger(c)$ together with coupling Hamiltonians of probe field and strong pump fields, which is given by total Hamiltonian of the field as

$$H_{field} = \hbar\omega_c c^\dagger c - i\hbar(c\varepsilon_p e^{i\omega_p t} - c^\dagger \varepsilon_p^\star e^{-i\omega_p t}) + i\hbar\varepsilon_l(ce^{i\omega_l t} - c^\dagger e^{-i\omega_l t}) \tag{2.2}$$

The hamiltonians for optomechanical coupling between cavity field and MR_1 are summed up as the total interaction Hamiltonian of the system which is given as

$$H_{int} = -g_0 c^\dagger c({b_1}^\dagger + b_1) \tag{2.3}$$

where, g_0 is optomechanical coupling strength which depends on the length of cavity and is given by $g_0 = (\frac{\omega_c}{L})\sqrt{\frac{\hbar}{2m_1\omega_1}}$.

The Hamiltonian for the external mechanical driving field of MR1, with amplitude ε_1 is given as

$$H_{dr} = i\hbar(\varepsilon_1 {b_1}^\dagger e^{-i\omega_1 t} - \varepsilon_1 b_1 e^{i\omega_1 t}) \tag{2.4}$$

The effective Hamiltonian describing this cavity based optomechanical system is yielded in a rotating frame at the frequency of strong pump laser field ω_l by

(for $\hbar = 1$)

$$H = H_0 + H_{int} + H_{fields} \tag{2.5}$$

where,

$$\begin{aligned} H_0 &= \Delta_c c^\dagger c \\ H_{int} &= -g_0 c^\dagger c({b_1}^\dagger + b_1) \\ H_{fields} &= i\varepsilon_1 {b_1}^\dagger e^{-i\delta t} + \varepsilon_l c^\dagger + \varepsilon_p c^\dagger e^{-i\delta t} - H.c \end{aligned}$$

Where $\Delta_c = \omega_c - \omega_l$. We suppose that the frequencies of the four driving fields satisfy the condition $\delta = \omega_p - \omega_l = \omega_1$.

2.2.2 Heisenberg-Langevin Equations of motion of the System

A strong laser field of frequency ω_l and a weak probe field of frequency ω_p are applied to the optical cavity and a switchable mechanical driving field of amplitudes ϵ_1 is applied to the mechanical resonators MR_1. The heisenberg-langevin equations of motion for the system can be calculated by using the standard relation

$$\frac{dO}{dt} = \frac{i}{\hbar}[H, O] - \frac{1}{2}\{\Gamma, O\} + N \tag{2.6}$$

O can be any operator of the system. First term gives the commutation relation between total energy of the system and operator of the system.Second term accounts for decays associated with that operator and the last term is noise operator, gives noise in the system.Now we write the equations of motion using equation (2.5) in (2.6)

$$\begin{aligned} \dot{c} &= -(i\Delta_c + \frac{\kappa}{2})c + ig_0({b_1}^\dagger + b_1)c + \varepsilon_l + \varepsilon_p e^{-i\delta t} + \sqrt{2\kappa}c_{in}(t) \\ \dot{b_1} &= -(i\omega_1 + \frac{\gamma_1}{2})b_1 + ig_0 c^\dagger c + \varepsilon_1 e^{-i\delta t} + \sqrt{2\gamma_1}\zeta_1(t) \end{aligned} \tag{2.7}$$

where $\Delta_c = \omega_c - \omega_l$, κ and γ_1 are decay terms related to cavity and mechanical resonators respectively. $c_{in}(t)$ is the input vacuum noise with zero mean value, $\zeta_1(t)$ and $\zeta_2(t)$ are the Brownian noise operators connected with the damping of the two mechanical resonators.Using Markov approximation, the correlation functions of these input noise operators are given by

$$\langle c_{in}(t)c_{in}(t')\rangle = \delta(t-t')$$

$$\langle \zeta_i(t)\zeta_i(t')\rangle = (n_{th}+1)\delta(t-t')$$

with $i = 1, 2$, here $n_{th} = (e^{\frac{\hbar\omega}{k_B T}} - 1)^{-1}$ and k_B is the Boltzmann constant and T is the temperature of the reservoir of the mechanical resonator.Using the mean-field approximation $\langle c^\dagger c\rangle \approx \langle c^\dagger\rangle\langle c\rangle$ to decouple the coupled operators, the equations of motion can be written as

$$\begin{aligned}
\langle \dot{c}\rangle &= -(i\Delta_c + \frac{\kappa}{2})\langle c\rangle + ig_0(\langle b_1\rangle^\dagger + \langle b_1\rangle)\langle c\rangle + \varepsilon_l + \varepsilon_p e^{-i\delta t} + \sqrt{2\kappa}\langle c_{in}(t)\rangle \\
\langle \dot{b_1}\rangle &= -(i\omega_1 + \frac{\gamma_1}{2})\langle b_1\rangle + ig_0\langle c^\dagger\rangle\langle c\rangle + \varepsilon_1 e^{-i\delta t} + \sqrt{2\gamma_1}\langle \zeta_1(t)\rangle
\end{aligned} \tag{2.8}$$

We are only concerned with the linear response of the nano-electro-optomechanical system to the weak probe field. We can neglect the noise terms associated with the system. So, in the case of ε_p, $\varepsilon_1 << \varepsilon_l$, we can linearize the dynamical equations of the proposed system by introducing small perturbations as $c = c_s + \delta c$ and $b_1 = b_{1s} + \delta b_1$. The steady state values of the system are found by setting the time derivative of the operators zero, in Eq(2.8).

$$\begin{aligned}
c_s &= \frac{\varepsilon_l}{i\Delta_c - ig_0({b_{1s}}^\dagger + b_{1s}) + \frac{\kappa}{2}} \\
b_{1s} &= \frac{ig_0|c_s|^2}{i\omega_1 + \frac{\gamma_1}{2}}
\end{aligned} \tag{2.9}$$

where c_s and b_{1s} are steady state values of cavity field photon number and phonon number of micro resonator MR1,respectively.

The fluctuation terms of the equations of motion can be reduced to

$$\begin{aligned} \delta\dot{c} &= -(i\Delta + \frac{\kappa}{2})\delta c + ig_0 c_s(\delta {b_1}^\dagger + \delta b_1) + \varepsilon_p e^{-i\delta t} \\ \delta\dot{b_1} &= -(i\omega_1 + \frac{\gamma_1}{2})\delta b_1 + ig_0 c_s \delta c^\dagger + ig_0 {c_s}^* \delta c + \varepsilon_1 e^{-i\delta t} \end{aligned} \tag{2.10}$$

where, $\Delta = \Delta_c - g_0({b_{1s}}^* + b_{1s})$ is the effective detuning.

To determine the amplitudes of first order side-bands in the system, we consider the following fluctuation terms

$$\begin{aligned} \delta c &= {A_1}^- e^{-i\delta t} + {A_1}^+ e^{i\delta t} \\ \delta b_1 &= {B_1}^- e^{-i\delta t} + {B_1}^+ e^{i\delta t} \end{aligned} \tag{2.11}$$

Substituting ansatz (2.11) into the set of equations (2.10), we get the following group of eight linear equations for first order sidebands

$$\begin{aligned} {h_1}^+ {A_1}^+ &= iG{B_1}^+ + iG{B_1}^{-*} + \varepsilon_p \\ {h_1}^- {A_1}^- &= iG{B_1}^- + iG{B_1}^{+*} \\ {h_2}^- {B_1}^+ &= iG{A_1}^{-*} + iG^* {A_1}^+ + \varepsilon_1 \\ {h_2}^+ {B_1}^- &= iG{A_1}^{+*} + iG^* {A_1}^- \\ {h_1}^+ {A_1}^{-*} &= -iG{B_1}^{-*} - iG{B_1}^+ \\ {h_1}^- {A_1}^{+*} &= -iG{B_1}^{+*} - iG{B_1}^- + \varepsilon_p \\ {h_2}^+ {B_1}^{+*} &= -iG{A_1}^{-*} - iG^* {A_1}^+ \\ {h_2}^- {B_1}^{-*} &= -iG{A_1}^{+*} - iG^* {A_1}^- + \varepsilon_1 \end{aligned} \tag{2.12}$$

where, $G = g_0 c_s$, ${h_1}^\pm = \pm i\Delta + \kappa/2 - i\delta$ and ${h_2}^\pm = \pm i\omega_1 + \gamma_1/2 - i\delta$.

By introducing the phase term ϕ_1 in the above set of equations as $\varepsilon_1 = \epsilon_1 e^{-i\phi_1}$ for external driving field ε_1, we can solve the system of equations for the value of ${A_1}^+$. It is obvious from above set of equations that ${A_1}^+$ is a function of weak

probe field frequency δ. By solving above set of equations in Eq. (2.12) leads to

$$A_1{}^+ = \frac{-2|G|^2(2G\varepsilon_1 e^{-i\phi_1} - ih_2{}^-\varepsilon_p)h_1{}^+}{h_1{}^+(2i|G|^2h_2{}^-h_1{}^+ - h_1{}^-(-2i|G|^2 + h_2{}^-h_1{}^+)h_2{}^+)} + \frac{(G^2h_1{}^-\varepsilon_p - (2iGh_1{}^-\varepsilon_1 e^{-i\phi_1} + (G^2 + h_1{}^-h_2{}^-)\varepsilon_p)h_1{}^+)h_2{}^+}{h_1{}^+(2i|G|^2h_2{}^-h_1{}^+ - h_1{}^-(-2i|G|^2 + h_2{}^-h_1{}^+)h_2{}^+)}. \tag{2.13}$$

2.3 Four-wave mixing (FWM)

Non-linearities arise in every system, when a high energy optical field is applied.In the context of cavity optomechanical system, non-linearities are present as in non-linear media,but the sources that produce these non-linearities in both cases are different.In basic cavity optomechanical systems, there is no medium inside the cavity but the non-linearities analogous to Kerr effect [12] are present. Such non-linear effects are due to radiation pressure force.As the radiation pressure force is changed with the oscillation of micro resonators, the non-linearity in the medium also is also changed with it.Due to non-linearity, the optical response of the optomechanical system is altered because of the mechanical interaction, and different phenomena like OMIT [13, 14, 15], and slow light effect [16] come into account. Four Wave Mixing is also one of those nonlinear effects investigated, as Huang and Agarwal [17]. Four-wave mixing (FWM) which has been under extensive research since the dawn of nonlinear optics, is one of the most prominent non-linear optical phenomenon based on quantum interference and coherence. This has potentially diverse applications, as frequency-conversion phenomenon [18], quantum-entanglement phenomenon [19], stopped light [20] and fast light [21]. Though, a comparatively small amount of the non-linear co-efficient can be taken into account by the loss of linear absorption in conventional materials. In order to overcome this hurdle, Harris. [22] presented that the third-order susceptibility can be resonantly enhanced using electromagnetically induced transparency (EIT) in a three-level system, which means that a highly efficient Four-wave mixing process

based on EIT is possible to be gained by reducing linear absorption. An experimental observation of the enhancement of non-degenerate Four-wave mixing based on EIT in a lambda-type three-level system of Rubidium atoms was made by Li and Xiao [23]. Wu et al. [24] showed that FWM can be enhanced by suppression of photon absorption from EIT in a five-level atomic system. Deng et al. [25] suggested a plan of action to open Four-wave mixing optical channels in a four-level system.

2.3.1 Calculation of FWM

The standard input-output relation is written as

$$\langle c_{out}(t)\rangle \;=\; (\varepsilon_l - \sqrt{2\kappa}c_s)e^{-i\omega_l t} + (\varepsilon_p - \sqrt{2\kappa}c_-)e^{-i\omega_p t} - \sqrt{2\kappa}c_+ e^{-i(2\omega_l-\omega_p)t}$$

Here we assume $c_- = {A_1}^-$ and $c_+ = {A_1}^+$. There are three components in the relation with frequencies ω_l, ω_p and $2\omega_l - \omega_p$. The third component with a newly generated frequency $2\omega_l - \omega_p$ corresponds to the Four-wave mixing (FWM), which is generated when two pump field photons combine with a probe field photon in the presence of optomechanical coupling. When there is no optomechanical coupling, there will be no four-wave mixing.The intensity of the four-wave mixing (FWM) is calculated by following relation

$$FWM \;=\; |-\frac{\sqrt{2\kappa}{A_1}^+}{\varepsilon_p}|^2. \tag{2.14}$$

2.4 Numerics and Results for Four-wave mixing (FWM)

For simulations, we choose experimental parameters for optomechanical system presented in [26].The length of cavity is taken $L = 25cm$ and other parameters are $g_0 = 2\pi \times 4kHz$, $\omega_1 = 2\pi \times 947kHz$, $\gamma_1 = 2\pi \times 140kHz$ and mass of the

micro-resonator MR1 is taken as $m_1 = 145ng$. As presented in [27] the cavity decay rate is $\kappa = 2\pi \times 215kHz$. The cavity field frequency is calculated by the relation $\omega_c = 2\pi c/\lambda_c$,where c is speed of light, and the value is calculated as $1.77 \times 10^{15} Hz$. We choose $\Delta_c = \omega_1$ and $\omega_l = \omega_c - \omega_1$, and the power of the pump field is taken as $9mW$. We consider the value of effective detuning to be $\Delta = \omega_1$. As we can see that the value of mechanical resonator frequency is greater than cavity decay rate, hence the system stays in the resolved sideband regime [28,29].

2.4.1 Coupling Controlled FWM in an optomechanical system

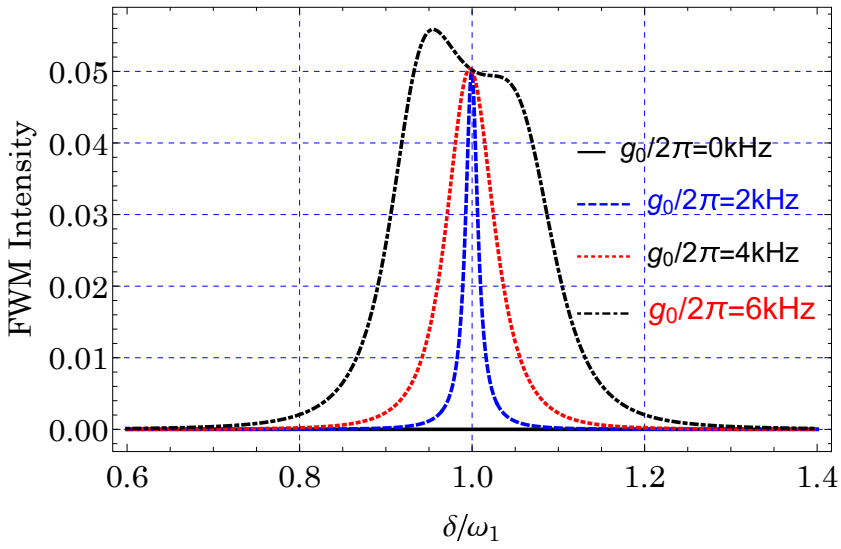

Figure 2.2: A 2-D plot for FWM Intesity (arbitrary units) vs normalized detuning δ/ω_1, for different values of optomechanical coupling strength g_0.The coulomb coupling parameter is kept zero, i.e $g_c = 0$. Other parameters are $\varepsilon_1 = 0$ and $\varepsilon_2 = 0$.

When the mechanical driving field is absent, i.e, $\varepsilon_1 = 0$, the FWM spectra consist of a single peak for lower optomechanical coupling values, as shown in Fig. 2.2. The peaks are located at Stokes ($\delta < \omega_1$) and Anti-Stokes ($\delta > \omega_1$) sideband regimes. It can be clearly observed that when the optomechanical coupling

is absent, there is no FWM signal in the output probe field [see, black dashed line in Fig. 2.2]. The FWM signal appears in the probe transmission field as optomechanical coupling is introduced (blue dashed line in Fig. 2.2) and the signal is amplified when the optomechanical coupling coefficient is increased [see, black dot-dashed curve in Fig. 2.2]. For lower optomechanical coupling strengths, the FWM curve consists of a single peak which is centered at $\delta = \omega_1$ [see blue dashed and red dotted curves]. This feature accounts for single photon resonance process [53]. For stronger optomechanical coupling strength, the curve becomes broadened and splits into two asymmetric peaks [see black dot-dashed line], thus producing two photons resonance process. The reason behind these features is explained as: When optomechanical coupling is increased, the cavity-mirror interaction becomes more stronger due to which more number of photons enter into the cavity which accounts for a stronger signal in the output field.

2.4.2 Phase Controlled FWM

We show the behavior of FWM intensity by keeping the optomechanical coupling strength constant and varying the amplitude and phase of external driving field ϵ_1. The value of coupling strength g_0 is taken as $2\pi \times 4kHz$.

In the presence of external driving field on micro-resonator MR_1 , the FWM peak can be suppressed at stokes sideband and amplified at anti-stokes sideband regimes.The intensity of FWM peak at anti-stokes sideband is smaller than the intensity of the peak at stokes sideband [see Fig. 2.3(a)]. With increasing the phase angle ϕ_1 of the driving field on MR_1 from 0 to $\pi/4$, the FWM spectra greatly increases for the peak at anti-stokes sideband but the signal is suppressed at the stokes sideband. This behavior is shown in Fig. 2.3(b).The reason behind these features is that the effective optomechanical coupling strength is enhanced due to the externally driven field.

In Fig. 2.4(a), for $\epsilon_1/\epsilon_p = 0.45$, the FWM intensity for the peak at stokes side-

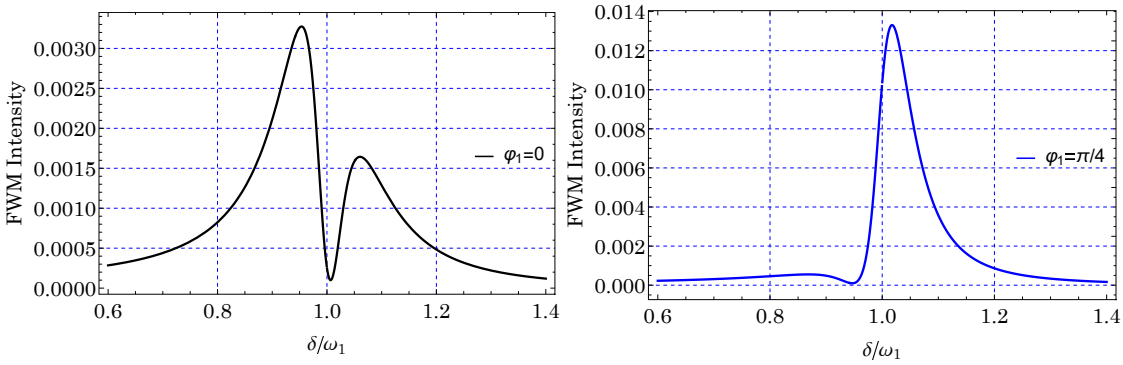

(a) (b)

Figure 2.3: FWM Intensity as a function of normalized detuning δ/ω_1. Only optomechanical coupling is present,and is kept constant,i.e, $g_0/2\pi = 4kHz$.The Coulomb coupling parameter is kept zero, i.e $g_c = 0$. Other parameters are $\varepsilon_1/\varepsilon_p = 0.45$ and $\varepsilon_2/\varepsilon_p = 0$. (a) $\phi_1 = 0$ and (b) $\phi_1 = \pi/4$.

band increases while decreases for the peak at anti-stokes side-band by setting the phase $\phi_1 = \pi$. The increase in phase angle ϕ_1 leads to a single peak ($\phi_1 = 3\pi/2$) at the resonance point, with increase in FWM intensity [see Fig. 2.4(b)].

As we further increase the phase angle, relative suppressions and amplifications

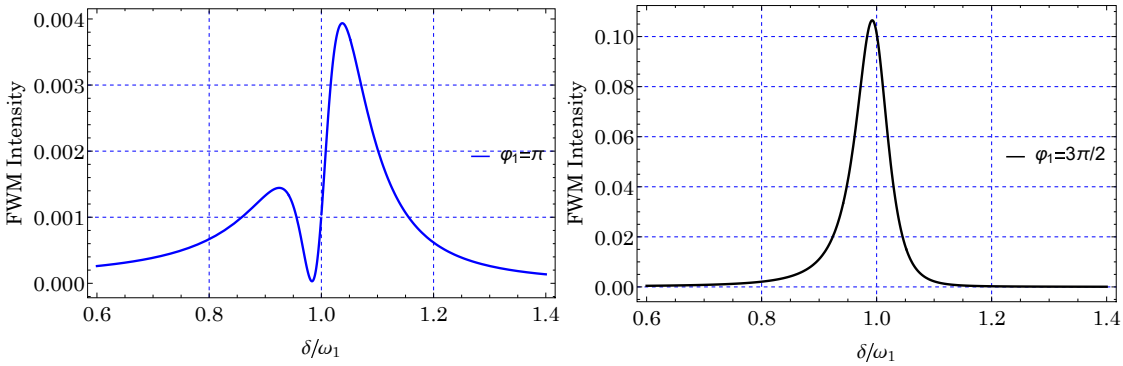

(a) (b)

Figure 2.4: FWM Intensity as a function of normalized detuning δ/ω_1. Other parameters are $\varepsilon_1/\varepsilon_p = 0.45$ and $\varepsilon_2/\varepsilon_p = 0$. (a) $\phi_1 = \pi$ and (b) $\phi_1 = 3\pi/2$.

of the FWM signal are appeared in the observed FWM spectra. This is due to

the fact that the effective optomechanical coupling coefficient is modified at every phase value.This periodic behavior is more clearly depicted in the Fig. 2.5. The

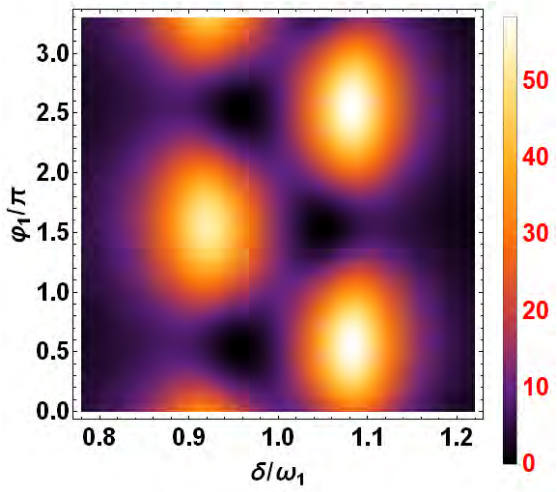

Figure 2.5: FWM Intensity as a function of normalized detuning δ/ω_1 and phase ϕ_1.Other parameters are $\varepsilon_1/\varepsilon_p = 0.45$ and $\varepsilon_2/\varepsilon_p = 0$.

FWM signal is strong at stokes line but the signal is very weak at anti-stokes line in the range of phase $\phi_1 = \pi$ to 2π, which can be clearly seen in Fig.2.5. These periodic amplification and suppression are observed in the intensity spots shown in Fig.2.5.

2.4.3 Amplitude controlled FWM signal

The amplification of the FWM signal is observed by varying the amplitude of the mechanical driving field at MR1.

The phase value is kept constant while investigating the effect of varying amplitude of mechanical driving on the FWM signal. From Fig. 2.6 , it can be seen that the intensity of FWM spectra prominently increases for both peaks, as well as the FWM near the resonance point becomes more stronger while in the absence of mechanical driving field, there was no FWM signal at the resonance point [see, Fig. 2.2].These features are due to the significant enhancement in the effective optomechanical coupling g_0. The optomechanical coupling strength g_0 plays a central

role in generating the FWM signal.The external mechanical driving field enhances the optomechanical coupling strength which accounts for a stronger FWM intensity in the output light signal. The intensity of both FWM peaks increases with

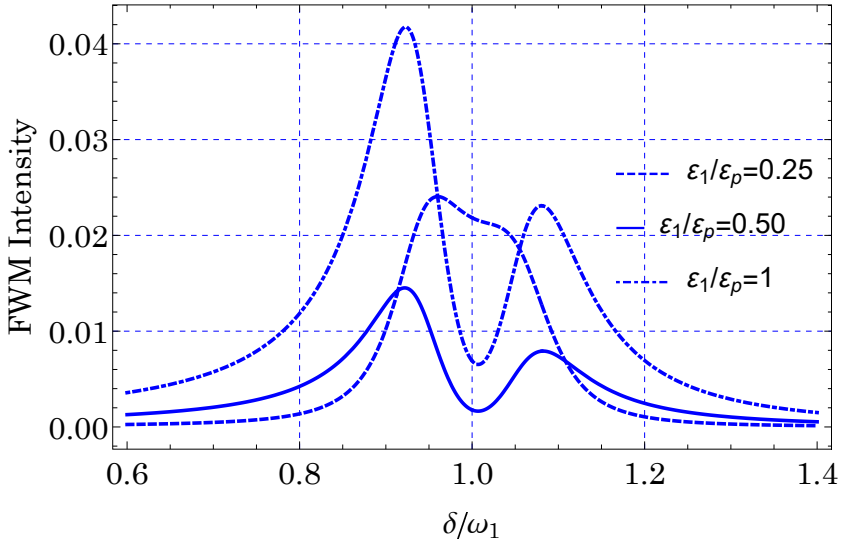

Figure 2.6: FWM Intensity as a function of normalized detuning δ/ω_1, for different values of $\varepsilon_1/\varepsilon_p$.

increase in the amplitude of external mechanical driving of MR1. For the amplitude $\epsilon_1/\epsilon_p = 0.25$, the FWM signal is absent at the off-resonance $\delta/\omega_1 = 1$ [see blue dashed curve]. When the amplitude of driving field at MR1 is increased, the FWM signal in the off-resonance regime prominently increases [see blue line and dot-dashed curves].

Chapter 3

Controlled FWM in a Nano Electro Optomechanical system

In this chapter, a new class of quantum hybrid system known as Nano Electro Optomechanical system (NEOMS) is discussed in the context of quantum optics.This system couples the optical, electrical and mechanical degrees of freedom in a single nano-scale device, a Nano transducer [63,65].

3.1 System Model

A typical Nano Electro Optomechanical system (NEOMS) is shown in Fig. 3.1, which is composed of a fixed mirror and a vibrating end mirror that combine to form an optomechanical system.The mechanical resonator MR1 is coupled to the cavity field via radiation pressure force.A second mirror (mechanical resonator MR2) is provided to the cavity which is coupled to the mechanical resonator MR1 through position-position coupling.

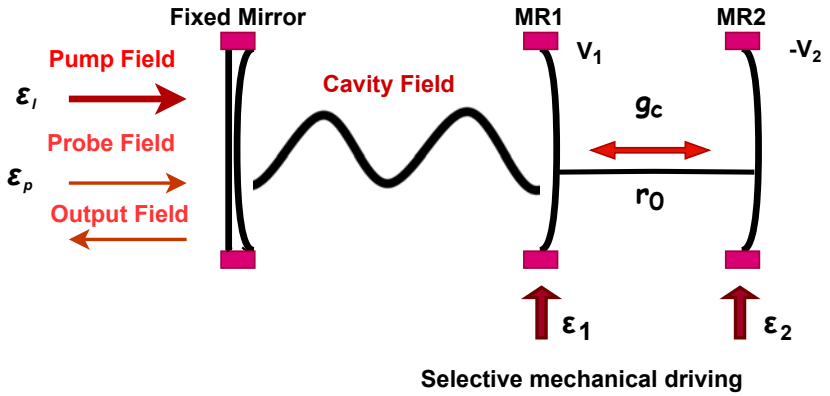

Figure 3.1: Schematic representation of the Nanoelectro-optomechanical system: MR_1 is coupled with the cavity field through optomechanical coupling g_0 and to the second mechanical resonator MR_2 through the Coulomb coupling strength g_c. A strong pump field ϵ_l and a weak probe field ϵ_p is fed to the cavity. MR_1 is charged by biased by V_1 and MR_2 is charged by $-V_2$. r_0 is the equilibrium distance. MR_s are selectively driven by ϵ_1 and ϵ_2.

The second mirror gives an additional control over the cavity field and it provides a versatile route to understand the nonlinear phenomena of cavity based electro-optomechanical systems.

3.2 Total Hamiltonian of the system

We consider single mechanical mode for vibrating end mirrors, modeled as harmonic oscillators MR_1 and MR_2 with frequencies ω_1 and ω_2 respectively, therefore the Hamiltonian of the mechanical oscillators is given by

$$H_{MRs} = \hbar\omega_1 {b_1}^\dagger b_1 + \hbar\omega_2 {b_2}^\dagger b_2 \tag{3.1}$$

where ω_1 and ω_2 are frequencies and $({b_1}^\dagger)$ b_1 and $({b_2}^\dagger)$ b_2 are (annihilation)creation operators of MR_1 and MR_2 respectively with $[b_i, {b_i}^\dagger] = 1$.

We are interested in the free Hamiltonian for the cavity with frequency ω_c and

bosonic creation(annihilation) operators $c^{\dagger}(c)$ together with coupling Hamiltonians of probe field and strong pump fields, which is given by total Hamiltonian of the field as

$$H_{field} = \hbar\omega_c c^{\dagger}c - i\hbar(c\epsilon_p e^{i\omega_p t} - c^{\dagger}\epsilon_p^{\star}e^{-i\omega_p t}) + i\hbar\epsilon_l(ce^{i\omega_l t} - c^{\dagger}e^{-i\omega_l t}) \quad (3.2)$$

The hamiltonians for optomechanical coupling between cavity field and MR_1, and the coulomb coupling between MR_1 and MR_2 are summed up as the total interaction Hamiltonian of the system which is given as

$$H_{int} = -g_0 c^{\dagger}c({b_1}^{\dagger} + b_1) + \hbar g_c({b_1}^{\dagger}b_2 + b_1{b_2}^{\dagger}) \quad (3.3)$$

where, g_0 is optomechanical coupling coefficient and its value is given by $g_0 = (\frac{\omega_c}{L})\sqrt{\frac{\hbar}{2m_1\omega_1}}$ and g_c is coulomb coupling strength and is given by $g_c = \frac{k_e q_1 q_2}{{r_0}^3}\sqrt{\frac{\hbar}{2m_1 m_2\omega_1\omega_2}}$ [54,55].

The Hamiltonians for the two external mechanical driving fields with amplitudes ϵ_1 and ϵ_2 are given as

$$H_{dr} = i\hbar(\epsilon_1{b_1}^{\dagger}e^{-i\omega_1 t} - \epsilon_1 b_1 e^{i\omega_1 t}) + i\hbar(\epsilon_2{b_2}^{\dagger}e^{-i\omega_2 t} - \epsilon_2 b_2 e^{i\omega_2 t}) \quad (3.4)$$

The effective Hamiltonian describing this Nano Electro Optomechanical system is yielded in a rotating frame at the frequency of strong pump laser field ω_l by (for $\hbar = 1$)

$$H = H_0 + H_{coup} + H_{fields} \quad (3.5)$$

where,

$$\begin{aligned} H_0 &= \Delta_c c^{\dagger}c \\ H_{coup} &= -g_0 c^{\dagger}c({b_1}^{\dagger} + b_1) + g_c({b_1}^{\dagger}b_2 + b_1{b_2}^{\dagger}) \\ H_{fields} &= i(\sum_{j=1}^{2}\epsilon_j{b_j}^{\dagger}e^{-i\delta t} + \epsilon_l c^{\dagger} + \epsilon_p c^{\dagger}e^{-i\delta t} - H.c) \end{aligned}$$

Where $\Delta_c = \omega_c - \omega_l$. We suppose that the frequencies of the four driving fields satisfy the condition $\delta = \omega_p - \omega_l = \omega_1 = \omega_2$

3.2.1 Heisenberg-Langevin Equations of motion of the System

A strong laser field of frequency ω_l and a weak probe field of frequency ω_p are applied to the optical cavity and two external driving fields of amplitudes ϵ_1 and ϵ_2 are applied to the mechanical resonators MR_1 and MR_2 respectively. The heisenberg-langevin equations of motion for the system can be calculated by using the standard relation

$$\frac{dO}{dt} = \frac{i}{\hbar}[H, O] - \frac{1}{2}\{\Gamma, O\} + N \tag{3.6}$$

O can be any operator of the system. First term gives the commutation relation between total energy of the system and operator of the system.Second term accounts for decays associated with that operator and the last term is noise operator, gives noise in the system.Now we write the equations of motion using Eq. 3.5 in Eq. 3.6 as

$$\begin{aligned}
\dot{c} &= -(i\Delta_c + \frac{\kappa}{2})c + ig_0(b_1{}^\dagger + b_1)c + \epsilon_l + \epsilon_p e^{-i\delta t} + \sqrt{2\kappa}c_{in}(t) \\
\dot{b_1} &= -(i\omega_1 + \frac{\gamma_1}{2})b_1 + ig_0 c^\dagger c - ig_c b_2 + \epsilon_1 e^{-i\delta t} + \sqrt{2\gamma_1}\zeta_1(t) \\
\dot{b_2} &= -(i\omega_2 + \frac{\gamma_2}{2})b_2 - ig_c b_1 + \epsilon_2 e^{-i\delta t} + \sqrt{2\gamma_2}\zeta_2(t)
\end{aligned} \tag{3.7}$$

where $\Delta_c = \omega_c - \omega_l$, κ and $\gamma_i (i = 1, 2)$ are decay terms related to cavity and mechanical resonators respectively. $c_{in}(t)$ is the input vacuum noise with zero mean value, $\zeta_1(t)$ and $\zeta_2(t)$ are the Brownian noise operators connected with the damping of the two mechanical resonators.Using Markov approximation, the correlation functions of these input noise operators are given by

$$\langle c_{in}(t)c_{in}(t')\rangle = \delta(t - t')$$

$$\langle \zeta_i(t)\zeta_i(t')\rangle = (n_{th} + 1)\delta(t - t')$$

with $i = 1, 2$, here $n_{th} = (e^{\frac{\hbar\omega}{k_B T}} - 1)^{-1}$ and k_B is the Boltzmann constant and T is the temperature of the reservoir of the mechanical resonator.Using the mean-field

approximation $\langle c^\dagger c\rangle \approx \langle c^\dagger\rangle\langle c\rangle$ to decouple the coupled operators, the equations of motion can be written as

$$\begin{aligned}
\langle\dot{c}\rangle &= -(i\Delta_c + \frac{\kappa}{2})\langle c\rangle + ig_0(\langle b_1\rangle^\dagger + \langle b_1\rangle)\langle c\rangle + \epsilon_l + \epsilon_p e^{-i\delta t} + \sqrt{2\kappa}\langle c_{in}(t)\rangle \\
\langle\dot{b_1}\rangle &= -(i\omega_1 + \frac{\gamma_1}{2})\langle b_1\rangle + ig_0\langle c^\dagger\rangle\langle c\rangle - ig_c\langle b_2\rangle + \epsilon_1 e^{-i\delta t} + \sqrt{2\gamma_1}\langle\zeta_1(t)\rangle \\
\langle\dot{b_2}\rangle &= -(i\omega_2 + \frac{\gamma_2}{2})\langle b_2\rangle - ig_c\langle b_1\rangle + \epsilon_2 e^{-i\delta t} + \sqrt{2\gamma_2}\langle\zeta_2(t)\rangle
\end{aligned} \tag{3.8}$$

We are only concerned with the linear response of the Nano Electro Optomechanical system to the weak probe field. We can neglect the noise terms associated with the system. So, in the case of ϵ_p, $\epsilon_{1,2} << \epsilon_l$, we can linearize the dynamical equations of the proposed system by introducing small perturbations as $c = c_s + \delta c$ and $b = b_{is} + \delta b_i$ $(i = 1, 2)$. The steady state values of the system are found by setting the time derivative of the operators zero, in Eq. 3.8.

$$\begin{aligned}
c_s &= \frac{\epsilon_l}{i\Delta_c - ig_0({b_{1s}}^\dagger + b_{1s}) + \frac{\kappa}{2}} \\
b_{1s} &= \frac{ig_0|c_s|^2 - ig_c b_{2s}}{i\omega_1 + \frac{\gamma_1}{2}} \\
b_{2s} &= \frac{-ig_c b_{1s}}{i\omega_2 + \frac{\gamma_2}{2}}
\end{aligned} \tag{3.9}$$

where c_s and $b_{is}(i = 1, 2)$ are steady state values of cavity field and micro resonators,respectively.

The fluctuation terms of the equations of motion can be reduced to

$$\begin{aligned}
\delta\dot{c} &= -(i\Delta + \frac{\kappa}{2})\delta c + ig_0 c_s(\delta {b_1}^\dagger + \delta b_1) + \epsilon_p e^{-i\delta t} \\
\delta\dot{b_1} &= -(i\omega_1 + \frac{\gamma_1}{2})\delta b_1 + ig_0 c_s \delta c^\dagger + ig_0 {c_s}^* \delta c - ig_c \delta b_2 + \epsilon_1 e^{-i\delta t} \\
\delta\dot{b_2} &= -(i\omega_2 + \frac{\gamma_2}{2})\delta b_2 - ig_c \delta b_1 + \epsilon_2 e^{-i\delta t}
\end{aligned} \tag{3.10}$$

where, $\Delta = \Delta_c - g_0({b_{1s}}^* + b_{1s})$ is the effective detuning.

To determine the amplitudes of first order side-bands in the system, we consider the following fluctuation terms

$$\delta c = {A_1}^- e^{-i\delta t} + {A_1}^+ e^{i\delta t}$$

$$\delta b_1 = {B_1}^- e^{-i\delta t} + {B_1}^+ e^{i\delta t}$$

$$\delta b_2 = {B_2}^- e^{-i\delta t} + {B_2}^+ e^{i\delta t} \tag{3.11}$$

Substituting ansatz (3.11) into the set of equations (3.10), we get the following group of eight linear equations for first order sidebands

$$\begin{aligned}
{h_1}^+ {A_1}^+ &= iG{B_1}^+ + iG{B_1}^{-*} + \epsilon_p \\
{h_1}^- {A_1}^- &= iG{B_1}^- + iG{B_1}^{+*} \\
k^+ {B_1}^+ &= iG{A_1}^{-*} + iG^* {A_1}^+ + \epsilon_1 - f\epsilon_2 \\
k^- {B_1}^- &= iG{A_1}^{+*} + iG^* {A_1}^- \\
{h_1}^+ {A_1}^{-*} &= -iG{B_1}^{-*} - iG{B_1}^+ \\
{h_1}^- {A_1}^{+*} &= -iG{B_1}^{+*} - iG{B_1}^- + \epsilon_p \\
{h_2}^+ {B_1}^{+*} &= -iG{A_1}^{-*} - iG^* {A_1}^+ + s{B_1}^+ + f\epsilon_2 \\
{h_2}^- {B_1}^{-*} &= -iG{A_1}^{+*} - iG^* {A_1}^- + t{B_1}^- + \epsilon_1
\end{aligned} \tag{3.12}$$

where, $G = g_0 c_s$, ${h_1}^\pm = \pm i\Delta + \kappa/2 - i\delta$, ${h_2}^\pm = \pm i\omega_1 + \gamma_1/2 - i\delta$, ${h_3}^\pm = \pm i\omega_2 + \gamma_2/2 - i\delta$, $k^\pm = {h_2}^\pm + {g_c}^2/{h_3}^\pm$, $s = {g_c}^2/{h_3}^+$, $t = {g_c}^2/{h_3}^-$ and $f = ig_c/{h_3}^+$.

By introducing the phase terms in the above set of equations as $\epsilon_1 = \epsilon_1 e^{-i\phi_1}$ and $\epsilon_2 = \epsilon_2 e^{-i\phi_2}$ for external driving fields ϵ_1 and ϵ_2 respectively , we can solve the system of equations for the value of ${A_1}^+$.

Solving the system of Eq. 3.12 for ${A_1}^+$, we find

$$\begin{aligned}
{A_1}^+ = &\frac{[2i|G|^2(sk^- - st + {h_2}^- {h_2}^+ + k^+ {h_2}^+) - k^- {h_1}^- {h_2}^+ ({h_2}^- + k^+)]G}{4i|G|^4(t-k^-)(s-k^+) + {h_2}^- {h_2}^+ (2|G|^2 + ik^- {h_1}^-)(k^+ {h_1}^+ - 2i|G|^2)}\epsilon_1 \\
&+ \frac{[2if|G|^2(st - sk^- - tk^+ + k^- k^+ - {h_2}^- {h_2}^+) + fk^- {h_1}^- {h_2}^- {h_2}^+]G}{4i|G|^4(t-k^-)(s-k^+) + {h_2}^- {h_2}^+ (2|G|^2 + ik^- {h_1}^-)(k^+ {h_1}^+ - 2i|G|^2)}\epsilon_2 \\
&+ \frac{[2|G|^2(st - sk^- - tk^+ + k^- k^+ - {h_2}^- {h_2}^+)]G^2}{4i|G|^4(t-k^-)(s-k^+) + {h_2}^- {h_2}^+ (2|G|^2 + ik^- {h_1}^-)(k^+ {h_1}^+ - 2i|G|^2)}\epsilon_p \\
&+ \frac{ik^+ {h_2}^+ (k^- - t)G^2 + {h_2}^- {h_2}^+ (2|G|^2 k^+ + ik^- {h_1}^- k^+ - iG^2 k^- {h_1}^-)}{4i|G|^4(t-k^-)(s-k^+) + {h_2}^- {h_2}^+ (2|G|^2 + ik^- {h_1}^-)(k^+ {h_1}^+ - 2i|G|^2)}\epsilon_p
\end{aligned}$$

3.3 Simulations

We numerically study the periodic suppressions and amplifications in FWM signal by choosing experimental parameters for a Nano Electro Optomechanical system presented in [26,27].The length of cavity is taken $L = 25cm$ and other parameters are $g_0 = 2\pi \times 4kHz$, $g_c = 0.2MHz$, $\omega_{1,2} = 2\pi \times 947kHz$, $\gamma_{1,2} = 2\pi \times 140kHz$ and masses of the micro-resonator MR1 are taken as $m_{1,2} = 145ng$. As presented in [27] the cavity decay rate is $\kappa = 2\pi \times 215kHz$. The cavity field frequency is calculated by the relation $\omega_c = 2\pi c/\lambda_c$,where c is speed of light, and the value is calculated as $1.77 \times 10^{15} Hz$. We choose $\Delta_c = \omega_1$ and $\omega_l = \omega_c - \omega_1$, and the power of the pump field is taken as $9mW$. We consider the value of effective detuning to be $\Delta = \omega_1$. As we can see that the values of mechanical resonator frequencies are greater than cavity decay rate,i.e $\omega_{1,2}$¿κ, hence the system stays in the resolved sideband regime [28,29].

3.3.1 FWM signal in the probe transmission field

The FWM signal in the output field is calculated using the relation from Eq. 2.14, which follows as

$$FWM \quad = \quad |-\frac{\sqrt{2\kappa}{A_1}^{+}}{\epsilon_p}|^2. \tag{3.13}$$

3.3.2 Coulomb coupling dependent FWM signal

In the absence of switchable mechanical driving fields at MRs, the FWM intensity is observed to show consistent amplifications and modifications.

Keeping the optomechanical coupling coefficient constant, i.e $g_0 = 2\pi \times 4kHz$, the FWM spectra is shown in Fig. 3.2 for different values of electrostatic Coulomb coupling strength g_c. The FWM spectra consists of two mode-splitting peaks.The

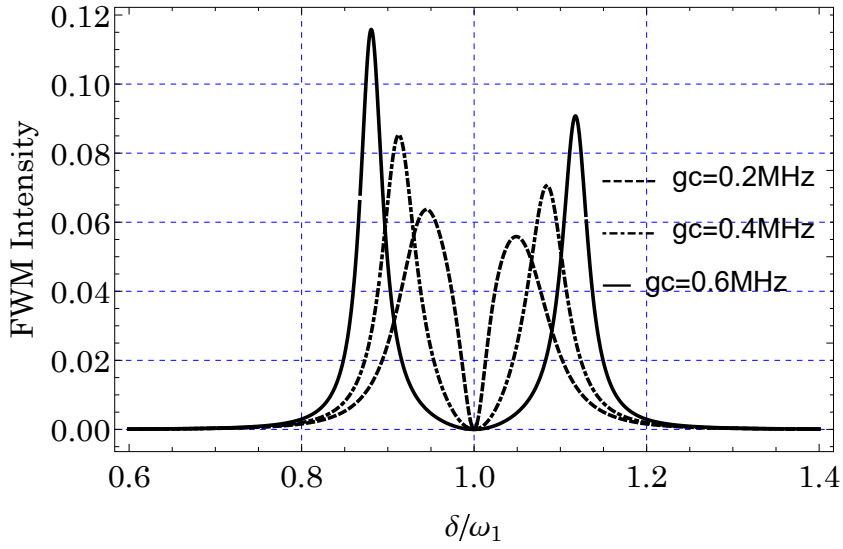

Figure 3.2: A 2-D plot for FWM Intesity (arbitrary units) vs normalized detuning δ/ω_1, for different values of g_c. Other parameters are $g_0/2\pi = 4kHz$, and $\varepsilon_1 = \varepsilon_2 = 0$..

intensity of peaks are almost same for lower values of Coulomb coupling (g_c) [see,dashed and dot-dashed black curves in Fig. 3.2] but intensity is different for higher values of g_c [see, black curve in Fig. 3.2]. An another prominent effect by the additional control of second mirror (MR2) kicks in, i.e the frequency shift between the two peaks.This frequency shift increases for higher values of g_c. The line width of both FWM peaks (at stokes and anti-stokes lines) decreases as the Coulomb coupling is increased.

These features are more clearly shown in a 3-D representation, as depicted in Fig. 3.3.

In Fig. 3.3, two intensity streams, separated by the frequency shift are clearly seen. Resonances, which are responsible for the FWM signal, appear in the regions of these bright bands. The FWM signal is absent in between (off-resonant points) these intensity streams.

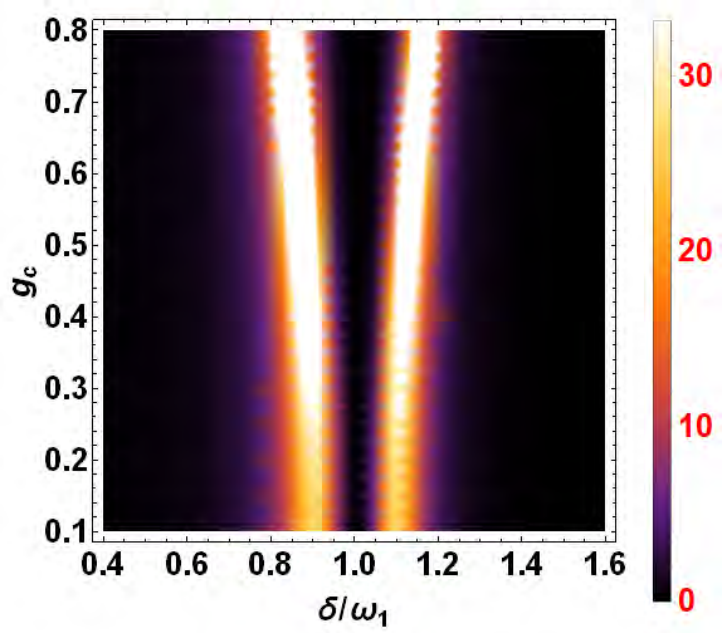

Figure 3.3: A 3-D plot for FWM Intesity (arbitrary units) as a function of normalized detuning δ/ω_1 and Coulomb coupling g_c.

3.3.3 Phase Controlled FWM signal

The versatile phase control gives intuitive understanding of the nonlinearities in cavity optomechanical systems. The extra control provided by the second mirror (MR2) can be appraised by varying the phases of the selective mechanical driving fields of MRs.

By only driving the second mirror (MR2) mechanically, i.e $\epsilon_1/\epsilon_p = 0$ and $\epsilon_2/\epsilon_p = 0.45$, two mode-splitting peaks are formed in the FWM spectra, which is shown in Fig. 3.4. In both peaks an asymmetrically amplified FWM signal is achieved [see, blue-dashed and black curves in Fig.3.4]. The FWM signal is suppressed ($\phi_2 = \pi/4$) and amplified ($\phi_2 = \pi$) at anti-stokes line while the light signal is amplified ($\phi_2 = \pi/4$) and suppressed ($\phi_2 = \pi$) at stokes line.The physics behind this asymmetric amplification and suppression can be explained as follows: In this system, by driving the mechanical resonator MR2, only effective Coulomb coupling can be enhanced. That is why asymmetric amplification and suppression

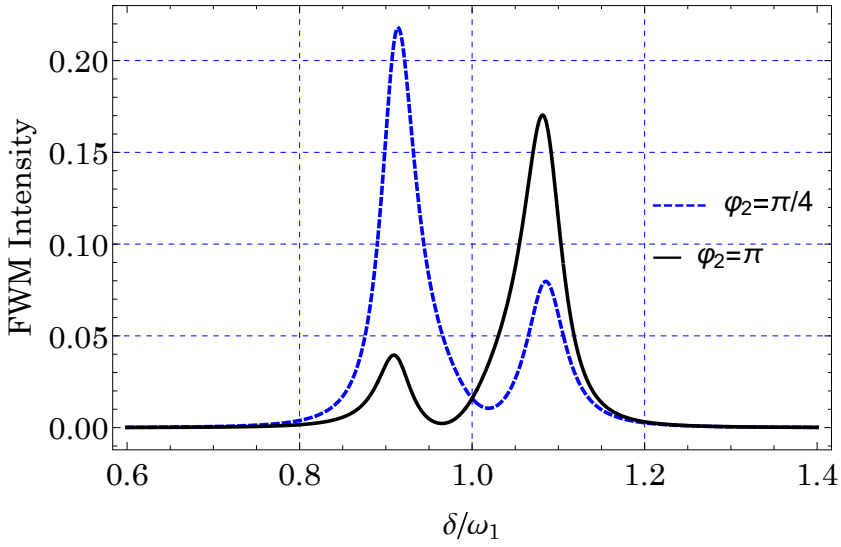

Figure 3.4: A 2-D plot for FWM Intesity (arbitrary units) as a function of normalized detuning δ/ω_1, for different values of ϕ_2. Other parameters are $g_0/2\pi = 4kHz$, $g_c = 0.4MHz$, $\varepsilon_1 = 0$, and $\varepsilon_2/\varepsilon_p = 0.45$.

of the FWM signal can be achieved by selective mechanical driving of MR2.

A 3-D representation of the phase controlled intensity of FWM signal is shown in Fig. 3.5. The amplification of FWM signal changes periodically with the phase ϕ_1 [see Fig. 3.5] by driving the mechanical resonator MR2 only. This asymmetric amplification of the light signal is due to enhancement in the effective Coulomb coupling. The FWM signal is absent in the off resonant region. Selective mechanical driving of both MRs, imparts the ability to completely block or amplify the FWM signal. To understand the FWM spectra in the presence of mechanical driving fields on both MRs,the amplitudes of both mechanical driving fields are set to $\epsilon_1/\epsilon_p = \epsilon_2/\epsilon_p = 0.45$. Asymmetric amplifications in the FWM light signal is achieved for the phase values $\phi_2 = 0$ and π, which is demonstrated in Fig.3.6. The mechanical driving of both MRs is advantageous at some extent because symmetric amplification can also be observed in the FWM signal [see blue-dashed curve in Fig.3.6]. A jitter variation (notch) in the FWM signal is found at the resonance point $\delta = \omega_1$. This feature is due to the fact that both effective optomechanical

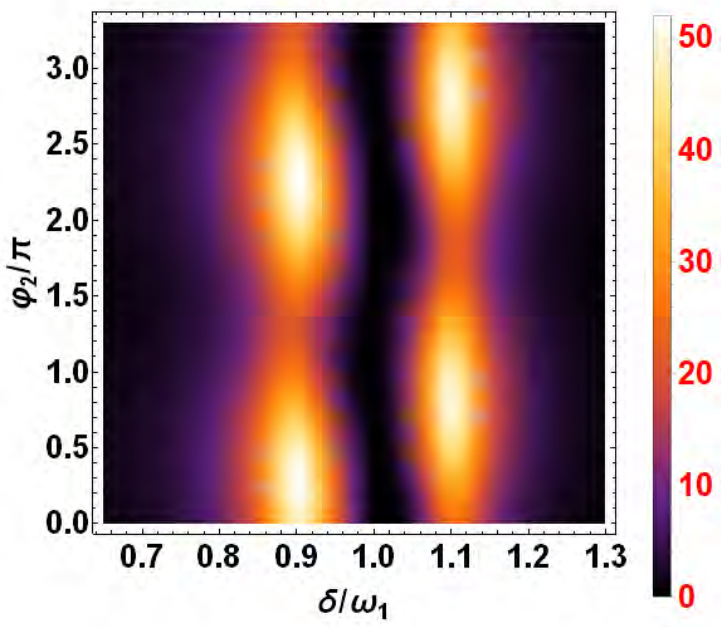

Figure 3.5: A 3-D plot for FWM Intesity (arbitrary units) as a function of normalized detuning δ/ω_1 and phase ϕ_2.

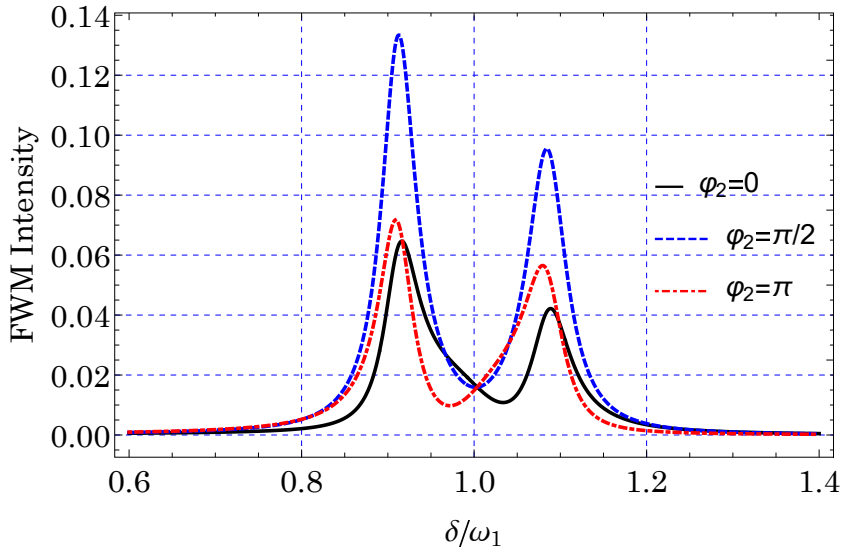

Figure 3.6: A 2-D plot for FWM Intesity (arbitrary units) as a function of normalized detuning δ/ω_1, for different values of ϕ_2. Other parameters are $g_0/2\pi = 4kHz$, $g_c = 0.4MHz$, $\varepsilon_1/\varepsilon_p = \varepsilon_2/\varepsilon_p = 0.45$.

coupling and Coulomb coupling strengths are enhanced by driving both MRs at the same time.

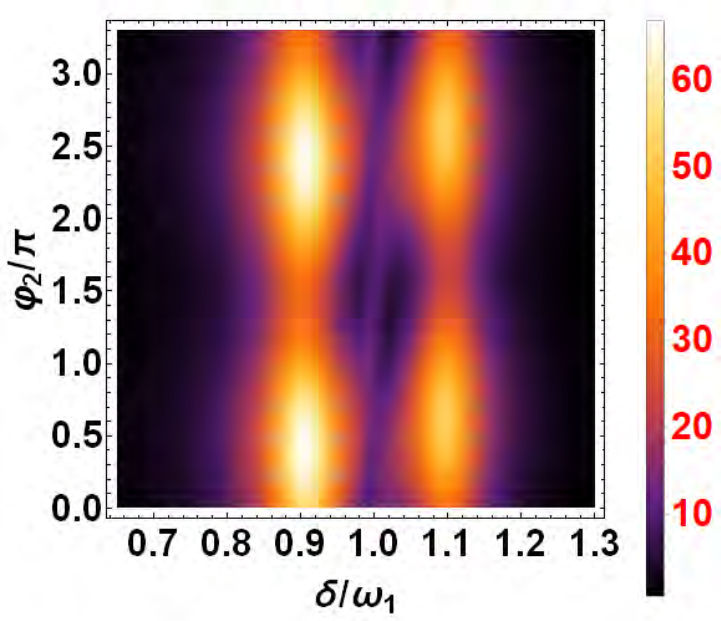

Figure 3.7: A 3-D plot for FWM Intesity (arbitrary units) as a function of normalized detuning δ/ω_1 and phase ϕ_2.

In the off resonant region ($\delta = \omega_1$), the FWM signal is not zero but has a weak signal in this area, as shown in Fig.3.7.

3.4 Amplitude Controlled FWM Spectra

In Fig.3.8 the FWM intensity is shown against the normalized detuning for varying amplitude of mechanical driving on MR2. Again asymmetric amplifications and suppressions are seen in the FWM signal around the resonance point. The FWM signal is almost blocked at the off resonant region $\delta = \omega_1$. This ability of selective switching and amplifying the input probe signal is highly desirable in practical optical communications [72-79].

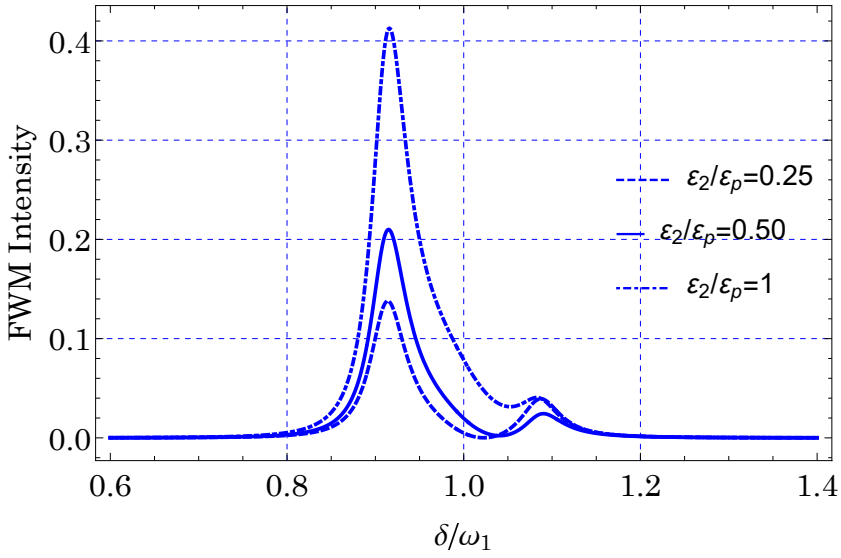

Figure 3.8: A 2-D plot for FWM Intesity (arbitrary units) as a function of normalized detuning δ/ω_1, for different values of $\varepsilon_2/\varepsilon_p$.

Chapter 4

Controlled FWM in NEOMS with Bose-Einstein Condensate

4.1 Basic Theory

Bose-Einstein condensation is a macroscopic occupation of atoms in a single quantum state. BEC was theoretically studied by Albert Einstein and Satyendra Nath Bose in 1924. BEC is formed when samples of bosons are trapped at temperatures near to absolute zero by different cooling techniques such as laser cooling [30], evaporative cooling [31] and magneto-optic trapping [32]. Experimentally, the pure Bose-Einstein condensate was observed in Rubidium-87 by Eric Cornell, Carl Weiman [33] and co-workers in June 1995., using a combination of laser cooling and magnetic-evaporative cooling [34,35]. Four months later, Wolfgang Ketterle [36] independently condensed Sodium-23 in MIT. In Lithium atoms BEC was observed by Randal Hullet [37] at Rice University. Many other groups are pursuing Bose-Einstein condensation by optical traps [38].

Electromagnetic Induced Transparency (EIT) [39,40] and Slow light [41,42,43] has been experimentally observed in Bose-Einstein condensate (BEC). Bose-Einstein condensate is an ideal test bed for EIT studies and Optical information processing.

4.2 Interatomic interaction in BEC

Several properties of Bose-Einstein condensate enter into the picture from the effects of atomic interactions. As we know that BEC is formed, when the de-Broglie wavelength of the atoms in the condensate is nearly approximate to the average inter-particle spacing.So, without working through detailed calculation, it is quite simple to understand the characterization of the scattering process by a single parameter, known as scattering length a.Normally, the chemical potential is effective across the distance of approximately $1nm$, and the de-Broglie wavelength is very large as 1000 times of the distance.This spells out that the collisions should be taken as diffracting waves from small obstacles.Therefore the dispersed field should consist of a spherical wave, which is only specified by its amplitude.This amplitude is actually the scattering length a. The condition for BEC to occur, with total number of trapped-atoms N, is

$$N(\frac{\hbar\omega}{k_B T})^3 = 1.2021$$

We notice that the condensate exists at temperature $700nK$, with approximately 10,000,000 atoms in the optical trap [65].

4.2.1 Nature of atom-atom interaction

In two atoms with cross wavefunctions, the inter-atomic interaction changes the energy of the atomic pair.This occurs due to a big amount of interaction energy when two atoms are closed to each other.The magnitude of energy shift depends on the scattering length a.If an atomic pair has an unperturbed energy E and the condensate is trapped in a volume of l^3 , its energy will be $E \approx \hbar^2/ml^2$. Therefore

$$\frac{\Delta E}{E} \approx N_0 \frac{a}{l} \tag{4.1}$$

where N_0 is the number of atoms. The dilute-gas condition, is therefore written as ${N_0}^{1/3} a/l << 1$.

The scattering length a can either be negative or positive. The negative sign indicates that the condensate has attractive interaction and the positive sign shows that the nature of interatomic interaction is repulsive.Rubidium condensate has repulsive interaction while Lithium has attractive interactions.By increasing N, the condensate will always reduce its energy by decreasing l which in turn rises the density and the condensate is no more a dilute gas.Another type of phase transition (liquid/solid) occurs instead of BEC.Hence, this limits the number of atoms N in a condensate with attractive interactions.

4.3 System Model

In this chapter we discuss the enhanced FWM signal in the presence of an atomic medium, i.e Bose-Einstein condensate (BEC). We explore the versatility of a trapped Bose-Einstein condensate (BEC) in a Nano Electro optomechanical system in the presence of switchable mechanical driving fields on mechanical resonators MR1 and MR2. The modifications in the intensity of FWM signal in the presence of atomic medium (BEC) will be studied numerically using suitable experimental parameters. A Nano Electro Optomechanical system (NEOMS) with a Bose-Einstein condensate trapped inside the optical cavity accompanied by the additional control of mechanical driving fields ε_1 and ε_2, is shown in Fig.4.1.

4.3.1 Mathematical Treatment

We assume that the atomic density is quite large that two body atom-atom interaction cannot be neglected and on-site kinetic energies and hopping of atoms are considerable. So we shall use Bose-Hubbard Model (BHM) [44], to fully describe the dynamics of Bose-Einstein condensate in NEOMS. From the microscopic

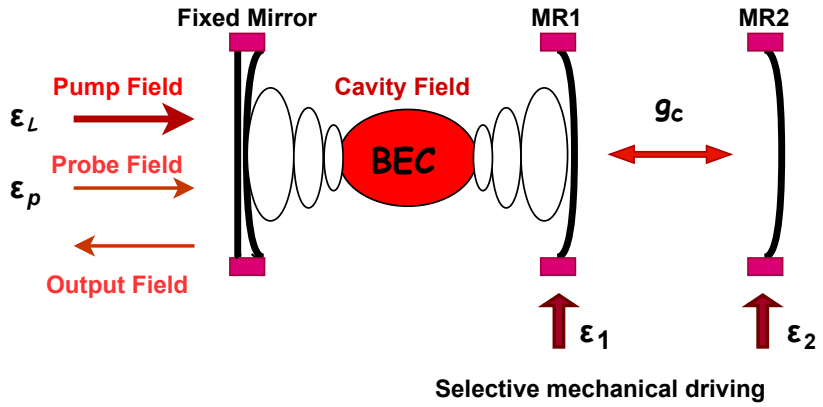

Figure 4.1: Schematic description of NEOMS with BEC trapped inside the optical cavity: MR_1 is coupled with the cavity through optomechanical coupling and optical field is coupled with two level N-atoms of BEC with atomic coupling stregnth g_a , and mechanical resonators MR_1 and MR_2 are coupled through the coulomb coupling strength g_c. ε_1 and ε_2 are external driving fields on MR_1 and MR_2 respectively.

second-quantized Hamiltonian,

$$H = \int dx\psi^\dagger(x)[-\frac{\hbar^2}{2m}\Delta^2 + V(x)]\psi(x) + \frac{\lambda}{2}\int d^3x\psi^\dagger(x)\psi^\dagger(x)\psi(x)\psi(x) \tag{4.2}$$

where, $\lambda = 4\pi a_{sc}\hbar^2/2m$ with a_s as s-wave scattering length and m is the mass of the condensate, and $V(x) = U_0 c^\dagger c\cos^2(kx)$ (here k is the wave number) with $U_0 = {g_a}^2/\Delta_a$ (here g_a is atomic coupling strength and Δ_a is the atomic detuning).

Now, expanding the field operators in terms of Wannier functions, i.e

$$\psi(x) = \sum_{i,n}\omega_n(x - x_i)b_i$$

we can write the optomechanical Bose-Hubbard Hamiltonian (OMBH) for the system presented in the work by assuming nearest neighbor approximation [45]

$$H_{BH} = \frac{U}{2}\sum_j({b_j}^\dagger {b_j}^\dagger b_j b_j) + \sum_j {b_j}^\dagger b_j(E_0 + \hbar U_0(V_{cl} + c^\dagger c)J_0) + \sum_j({b_{j+1}}^\dagger b_j + b_{j+1}{b_j}^\dagger)(E + \hbar U_0(V_{cl} + c^\dagger c)J) \tag{4.3}$$

The first term of Eq.4.3 represents the atom-atom interaction, second term is the hamiltonian of on-site kinetic energy and tunneling energy and the third term represents the tunneling (hopping) of atoms along the lattice sites. Where, U is two body atom-atom interaction energy,$b_j{}^\dagger(b_j)$ are bosonic creation(destruction) operators at the jth site, E_0 is the on-site kinetic energy, U_0 is the height of the optical lattice potential per photon, V_{cl} is the classical potential added to the system and J_0 is the tunneling energy. The relations for these terms are given as

$$\begin{aligned} U &= \frac{4\pi a_{sc}\hbar^2}{2m}\int d^3x|\omega(x-x_j)|^4, \\ E_0 &= \int d^3x\omega(x-x_j)(-\frac{\hbar^2\Delta^2}{2m})\omega(x-x_j), \\ J_0 &= \int d^3x\omega(x-x_j)\cos^2(kx)\omega(x-x_j), \\ U_0 &= \frac{{g_a}^2}{\Delta_a} \end{aligned} \tag{4.4}$$

We are using nearest neighbour approximation, so we can neglect the third term of Eq.4.2, and only considering the first two terms, the total Hamiltonian of the system in a rotating frame with laser frequency ω_l in the presence of input pump field ϵ_l, weak probe field ϵ_p and selective mechanical drivings of mechanical resonators MR_1 and MR_2, can be written as

$$\begin{aligned} H_T = \frac{U}{2}\sum_j(b_j{}^\dagger b_j{}^\dagger b_j b_j) + \sum_j b_j{}^\dagger b_j(E_0+\hbar U_0(V_{cl}+c^\dagger c)J_0) \\ +\Delta_c c^\dagger c - g_0 c^\dagger c(b_1{}^\dagger + b_1) + g_c(b_1{}^\dagger b_2 + b_1 b_2{}^\dagger) \\ +i(\sum_{k=1}^{2}\varepsilon_k b_k{}^\dagger e^{-i\delta t} + \varepsilon_l c^\dagger + \varepsilon_p c^\dagger e^{-i\delta t} - H.c) \end{aligned} \tag{4.5}$$

For a detailed investigation of dynamics of the system, photon losses are included along with the decay rate connected to the condensate, κ and γ_b respectively.So, the dynamics of the system is described by solving the Heisenberg-Langevin equations of motion, we get

$$\begin{aligned} \dot{c} &= -(i\Delta_c + \frac{\kappa}{2})c + ig_0(b_1{}^\dagger + b_1)c - iU_0J_0c\sum_j b_j{}^\dagger b_j + \varepsilon_l + \varepsilon_p e^{-i\delta t} + \sqrt{2\kappa}c_{IN} \\ \dot{b_j} &= -\frac{E_0}{\hbar}b_j - iJ_0[\frac{V_{cl}}{\hbar} + U_0c^\dagger c]b_j - i\frac{U}{\hbar}b_j{}^\dagger b_j b_j - \gamma_b b_j + \sqrt{2\gamma_b}b_{IN} \end{aligned}$$

Where, c_{IN} and b_{IN} are noise operators connected to the cavity-field and BEC, respectively.Using the ansatz $c = c_s + \delta c$ and $b = b_s + \delta b$, we can linearize the equations of motion. In case of negligible tunneling, we remove the site index j from the bosonic operators [45,46].Moreover we explicate the quadrature of mechanical mode of BEC by assuming Hermitian operators,that is, $\delta q = (\delta b + \delta b^\dagger)/\sqrt{2}$ and $\delta p = (\delta b - \delta b^\dagger)/i\sqrt{2}$. By excluding the quantum fluctuation terms averaged to zero [47,48], the linearized set of Heisenberg-Langevin equations of motion along with equations for mechanical resonators , is

$$\begin{aligned}
\delta\ddot{q} + \gamma_b\delta\dot{q} + {\omega_b}^2\delta q &= -gF(\delta c + \delta c^\dagger) \\
\delta\dot{c} &= -(\frac{\kappa}{2} + i\Delta)\delta c - igq + ig_0c_s(\delta {b_1}^\dagger + \delta b_1) + \varepsilon_l + \varepsilon_p e^{-i\delta t} \\
\delta\dot{b_1} &= -(i\omega_1 + \frac{\gamma_1}{2})\delta b_1 + ig_0c_s\delta c^\dagger + ig_0{c_s}^*\delta c - ig_c\delta b_2 + \varepsilon_1 e^{-i\delta t} \\
\delta\dot{b_2} &= -(i\omega_2 + \frac{\gamma_2}{2})\delta b_2 - ig_c\delta b_1 + \varepsilon_2 e^{-i\delta t} \qquad (4.6)
\end{aligned}$$

where, $\Delta = \Delta_c - U_0NJ_0 - g_0({b_{1s}}^\dagger + b_{1s}) + gq_s$ is the effective detuning, $g = 2U_0J_0\sqrt{N}|c_s|^2$, $F = U_{eff} + v$, $\omega_b = \sqrt{(F)(v + 3U_{eff})}$, $U_{eff} = \frac{UN}{\hbar M}$ and $v = U_0J_0|c_s|^2 + \frac{V_{cl}J_0}{\hbar} + \frac{E_0}{\hbar}$, (here N represents number of atoms in M sites).

To calculate the first order sidebands, we use the ansatz [49,50]

$$\begin{aligned}
\delta c &= {A_1}^- e^{-i\delta t} + {A_1}^+ e^{i\delta t} \\
\delta b_1 &= {B_1}^- e^{-i\delta t} + {B_1}^+ e^{i\delta t} \\
\delta b_2 &= {B_2}^- e^{-i\delta t} + {B_2}^+ e^{i\delta t} \\
\delta q &= E^- e^{-i\delta t} + E^+ e^{i\delta t}
\end{aligned}$$

Using above ansatz in the set of Eq.4.6, we get a system of twelve linear equations,

$$\begin{aligned}
-gF{A_1}^{+} - gF{A_1}^{-*} - {r_1}^{-}E^{+} &= 0 \\
-gF{A_1}^{-} - gF{A_1}^{+*} - {r_1}^{-}E^{-} &= 0 \\
{h_1}^{+}{A_1}^{+} - iG{B_1}^{+} - iG{B_1}^{-*} + igE^{+} &= 0 \\
{h_1}^{-}{A_1}^{+} - iG{B_1}^{-} - iG{B_1}^{+*} + igE^{-} &= \varepsilon_p \\
{h_1}^{+}{A_1}^{+*} + iG{B_1}^{-} + iG{B_1}^{+*} - igE^{-} &= 0 \\
{h_1}^{-}{A_1}^{-*} + iG{B_1}^{+} + iG{B_1}^{-*} - igE^{+} &= \varepsilon_p \\
-iG^{*}{A_1}^{+} - iG{A_1}^{-*} + {k_1}^{+}{B_1}^{+} + ig_c{B_2}^{+} &= 0 \\
-iG^{*}{A_1}^{+*} - iG^{*}{A_1}^{-} + {k_1}^{-}{B_1}^{-} + ig_c{B_2}^{-} &= \varepsilon_1 \\
iG{A_1}^{+*} + iG^{*}{A_1}^{-} - ig_c{B_2}^{-} + {k_1}^{+}{B_1}^{+*} &= 0 \\
iG^{*}{A_1}^{+} + iG{A_1}^{-*} - ig_c{B_2}^{+} + {k_1}^{-}{B_1}^{-*} &= 0 \\
{k_2}^{+}{B_2}^{+} + ig_c{B_1}^{+} &= 0 \\
{k_2}^{-}{B_2}^{-} + ig_c{B_1}^{-} &= \varepsilon_2
\end{aligned} \tag{4.7}$$

Here,

$$\begin{aligned}
G = g_0 c_s \quad ; \quad {h_1}^{\pm} &= \kappa/2 + i(\Delta \pm \delta) \\
{k_1}^{\pm} = \gamma_1/2 + i(\omega_1 \pm \delta) \quad ; \quad {k_2}^{\pm} &= \gamma_2/2 + i(\omega_2 \pm \delta) \\
G^{*} = g_0 {c_s}^{*} \quad ; \quad {r_1}^{\pm} &= {\omega_b}^2 - \delta^2 \pm i\delta\gamma_b
\end{aligned}$$

To understand the complete dynamics of medium (BEC) mediated FWM signal, phases for mechanical drivings ε_1 and ε_2 are introduced as,

$$\varepsilon_1 = \epsilon_1 e^{-i\phi_1} \;\; ; \;\; \varepsilon_2 = \epsilon_2 e^{-i\phi_2}$$

Solving the set of linear equations in Eq.4.7 for the first order sideband mode ${A_1}^{+}$, we get

$${A_1}^{+} = \frac{H_1}{C_1 + C_2 + C_3}\varepsilon_1 + \frac{H_2}{C_1 + C_2 + C_3}\varepsilon_2 + \frac{H_3}{C_1 + C_2 + C_3}\varepsilon_p \tag{4.8}$$

Where,

$$
\begin{aligned}
H_1 &= G({g_c}^2 + {k_1}^+{k_1}^-)(-2ig^2F + {h_1}^-{r_1}^-) \\
H_2 &= -Gg_c({k_1}^+ - {k_1}^-)(2g^2F + i{h_1}^-{r_1}^-) \\
H_3 &= -(g^2F{k_1}^+({g_c}^2 + {k_1}^-{k_2}^-) - iG({k_1}^+ - {k_1}^-){k_2}^-{r_1}^-G^*) \\
C_1 &= g^2F({g_c}^2({h_1}^+ + {h_1}^-){k_1}^+ - 2G^2{k_2}^-(({k_1}^+ - {k_1}^-) + ({h_1}^+ - {h_1}^-){k_1}^+{k_1}^-)) \\
C_2 &= i{h_1}^-({g_c}^2{h_1}^+{k_1}^+ + {h_1}^+{k_1}^+{k_1}^-{k_2}^- + G^2({k_1}^- - {k_1}^+){k_2}^-){r_1}^- \\
C_3 &= G({k_1}^+ - {k_1}^-){k_2}^-(2g^2F + i{h_1}^+{r_1}^-)G^*
\end{aligned}
$$

4.4 Numerical Results

We examine a repulsive Bose-Einstein condensate Rb^{87} of two level N-atoms and take data from real experiments [52,53]. We use experimental parameters to study enhancement in FWM signal in a Nano Electro Optomechanical system (NEOMS) in the presence of Bose-Einstein condensate (BEC) trapped inside the optical cavity. The experimental parameters for the Rb^{87} condensate [53] is given in the Table 4.1. Other parameters related to cavity field, coupling strengths and

Experimental parameters	
Parameters	Values
m_{bec}	$1.45 \times 10^{-25}kg$
a_{sc}	$109a_0$
ω	$38.628kHz$
N	$10^5 atoms$

Table 4.1: In the table, $a_0 = 0.529 \times 10^{-10}m$ is the Bohr radius.

mechanical resonators are same as in Section 3.3.

The FWM intensity is calculated using the relation,

$$FWM \quad = \quad |-\frac{\sqrt{2\kappa}}{\varepsilon_p} A_1{}^{+}|^2.$$

4.4.1 FWM signal for varying atom-field coupling g

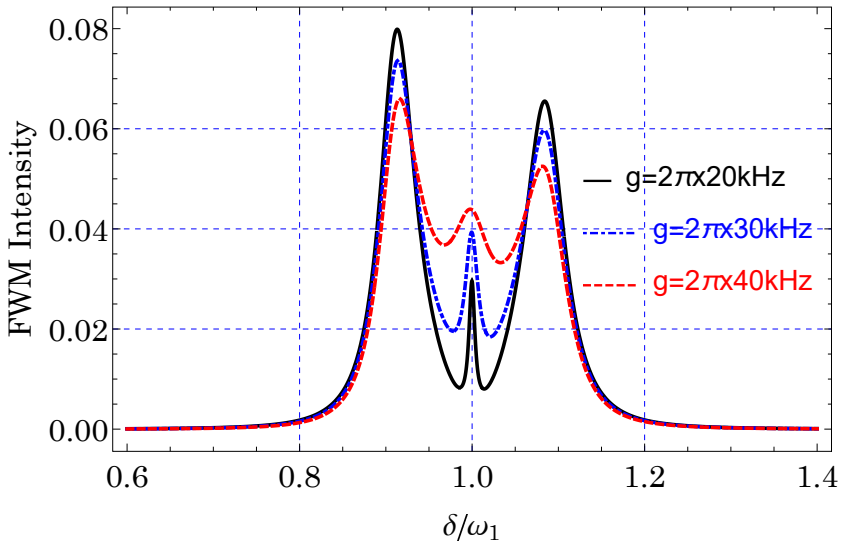

Figure 4.2: A 2-D plot for FWM Intesity (arbitrary units) as a function of normalized detuning δ/ω_1. Other parameters are $\omega_b = \omega_1$, $U_{eff} = v = \omega_b$, $\gamma_b = 0.01\gamma_1$, $\Delta_a = \omega_1$ and $\Delta = \omega_1$.

In the presence of an atomic medium, i.e, Bose Einstein Condensate (BEC), a third peak appears at the resonance point (δ/ω_1) in the FWM intensity curve, as shown in Fig 4.2. When the atom-field coupling is increased, three prominent changes occur in the FWM intensity; The FWM intensity decreases for the peaks right and left to the resonance point, the intensity of the new peak at the resonance point increases and the line-width of the peak at resonance point also increases [see blue-dotdashed and red-dotted curves in Fig 4.2]. These changes occur due to the following reason; When the atom-field coupling is increased, the non-linearity in the cavity is enhanced, which rigorously alters the output signal.

4.4.2 Phase controlled FWM Signal in the presence of atomic medium (BEC)

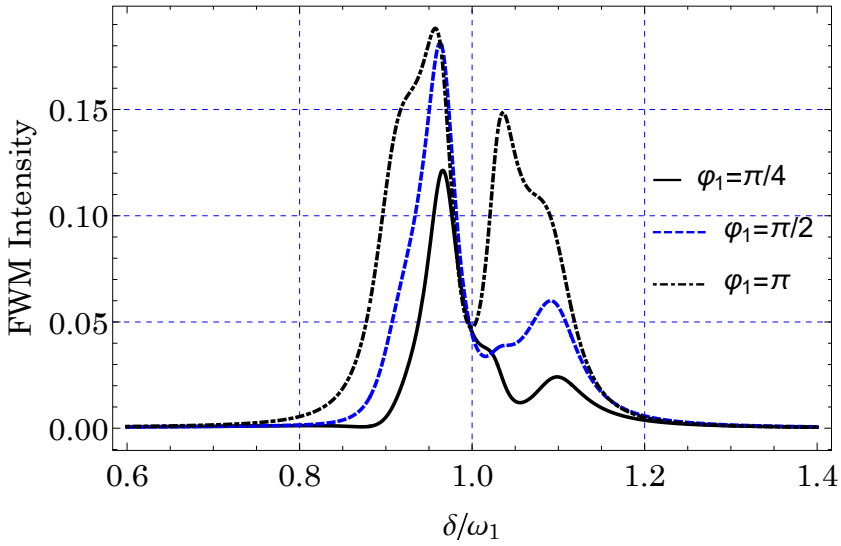

Figure 4.3: A 2-D plot for FWM Intesity (arbitrary units) as a function of normalized detuning δ/ω_1, for different values of phase angle ϕ_1. Other parameters are $g/2\pi = 30kHz$, $\varepsilon_1/\varepsilon_p = 0.45$, $\varepsilon_2/\varepsilon_p = 0$, $\omega_b = \omega_1$, $U_{eff} = v = \omega_b$, $\gamma_b = 0.01\gamma_1$, $\Delta_a = \omega_1$ and $\Delta = \omega_1$.

When the mechanical resonator MR_1 is driven, the FWM signal confronts to various modifications.As the phase angle ϕ_1 is increased, the intensities of FWM peaks on both sides of the resonance point (δ/ω_1) increase [see Fig.4.3]. The FWM signal strength at the resonance point is independent of the phase value, as shown in Fig 4.3. For lower phase values, the FWM signal right to the resonance point is suppressed [see black-dotted and blue-dashed curves in Fig 4.3]. When MR_1 is driven, the optomechanical coupling strength is enhanced, due to which consistent modifications occur in the output field. Because of this reason, asymmetric suppression and amplifications are observed in the FWM signal.

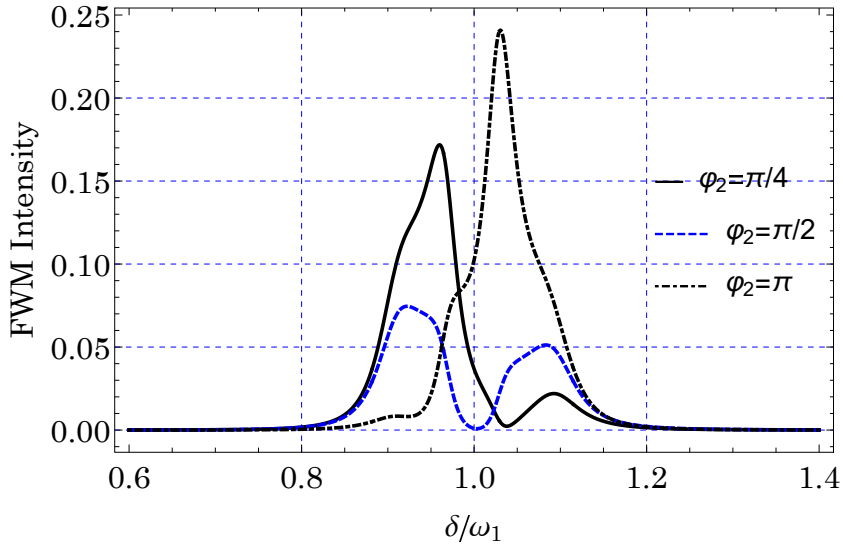

Figure 4.4: A 2-D plot for FWM Intesity (arbitrary units) as a function of normalized detuning δ/ω_1, for different values of phase angle ϕ_2. Other parameters are $g/2\pi = 30kHz$, $\varepsilon_1/\varepsilon_p = 0$, $\varepsilon_2/\varepsilon_p = 0.45$, $\omega_b = \omega_1$, $U_{eff} = v = \omega_b$, $\gamma_b = 0.01\gamma_1$, $\Delta_a = \omega_1$ and $\Delta = \omega_1$.

When the mechanical resonator MR_2 is driven instead of MR_1, anomalous changes occur in the FWM signal. At the phase angle $\phi_2 = \pi/4$, the amplitude of the FWM peak left to the resonance point δ/ω_1 is greater than that of the peak right to the resonance point [see black-line curve in Fig 4.4]. For the phase value $\phi_2 = \pi/2$, almost symmetric FWM peaks are observed around the resonance point δ/ω_1 [see blue-dashed curve in Fig 4.4]. At higher phase values, i.e $\phi_2 = \pi$, the FWM intensity of the peak right to the resonance point is greatly amplified while the FWM signal is almost absent at the left side of the resonance point [see black-dotdashed curve in Fig 4.4].

Chapter 5

Conclusion

In the first part of the dissertation, we investigate the phenomenon of four-wave mixing in an optomechanical system in the presence of a switchable mechanical driving field on the moving-end mirror (MR1). Asymmetric amplifications and suppressions have been observed in the output light signal (FWM).In addition, it has been shown that the FWM signal can be controlled by varying the amplitude and phase of mechanical driving on MR1.

The four-wave mixing phenomenon has been studied in a typical Nano Electro Optomechanical system (NEOMS), in the second part of the thesis. We show that the second micro resonator (MR2) provides an extra control over the FWM signal. It has been seen that the selective mechanical drivings of both MRs have a significant effect on the FWM spectra. These switchable mechanical drivings impart a tunable FWM signal at the output.Moreover, it has been observed that the intensities of FWM peaks can be amplified and suppressed by varying the amplitude and phase of mechanical drivings of MRs.

The last part of the dissertation discusses effect of atomic medium on the FWM signal. For this purpose a trapped Bose-Einstein condensate (BEC) in a Nano Electro Optomechanical system (NEOMS) has been studied by selectively driving the mechanical resonators MR1 and MR2. The medium-enhanced FWM

signal has been observed to show inconsistent modifications by varying the phase angle of mechanical driving fields of MRs. Moreover, it has been observed that the FWM signal can be greatly enhanced by driving the mechanical resonator (MR2) only.

Bibliography

[1] Gerry, Christopher, Knight and Peter, "Introduction to Quantum Optics", Cambridge University Press,(2004).

[2] M.P Blencowe, Phys. Rep. **395**, 159 (2004).

[3] K.C. Schwab and M.L. Roukes, Phys. Today **58**, 36 (2005).

[4] M.Aspelmeyer and K.Schwab, New J.Phys. **10** 095001 (2008).

[5] T.J Kippenberg and K.J. Vahala, Opt.Expr. **15**, 17172 (2007).

[6] Takesue, Hiroki and Inoue, Kyos, Phys. Rev. A. **70**, 031802 (2004).

[7] Phuc, N. T., Kawaguchi, Y. and Ueda, M. Phys. Rev. Lett. **113**, 230401 (2014).

[8] Yamamoto Y., Takahashi Y ,"Bose-Einstein Condensation: A Platform for Quantum Simulation Experiments", Springer, Tokyo (2016).

[9] Liu, Chien, Dutton, Zachary, Behroozi, Cyrus H., Hau, Lene Vestergaard, "Observation of coherent optical information storage in an atomic medium using halted light pulses", Nature. , 6819 (2001).

[10] Habel, F., Trubetskov, M., and Pervak, V., "Group delay dispersion measurements in the mid-infrared spectral range ", Optics express,**24**, 16705 (2016).

[11] Berges, J., Boguslavski, K., Chatrchyan, A., and Jaeckel, J. , Phys. Rev. D, **96**, 076020 (2017).

[12] Xiong, W., Jin, D. Y., Qiu, Y., Lam, C. H., and You, J. Q., Phys. Rev. A, **93**, 023844 (2016).

[13] Zhang, X. Y., Zhou, Y. H., Guo, Y. Q., and Yi, X. X. , Phys. Rev. A, **98**, 053802 (2018).

[14] Xiao, Y., Yu, Y. F., and Zhang, Z. M. , Optics express, **22**, 17989 (2014).

[15] Ivan Favero and Florian Marquardt, New Journal of Physics, Volume 16, (2014).

[16] Safavi-Naeini, A. H., Alegre, T. M., Chan, J., Eichenfield, M., Winger, M., Lin, Q., ... and Painter, O. , Nature, **69**, 7341 (2011).

[17] Huang, S., and Agarwal, G. S. , Phys. Rev. A, **81**, 033830 (2010).

[18] Jain M., Xia H., Yin G. Y., Merriam A. J. and Harris S. E., Phys. Rev. Lett., **77**, 6326 (1996).

[19] Payne M. G. and Deng L., Phys. Rev. Lett., **91**, 123602 (2003).

[20] Camacho R. M., Vudyasetu P. K. and Howell J. C., Nat. Photon., **3** ,103 (2009).

[21] Glasser R. T., Vogl U. and Lett P. D., Phys. Rev. Lett., **108**,173902 (2012).

[22] Harris S. E., Field J. E. and Imamoglu A. , Phys. Rev. Lett., **64**, 1107 (1990).

[23] Li Y. and Xiao M., Opt. Lett., **21**, 1064 (1996).

[24] Wu Y., Saldana J. and Zhu Y. F., Phys. Rev. A, **67**, 013811 (2003).

[25] Deng L., Kozuma M., Hagley E. W. and Payne M. G., Phys. Rev. Lett., **88**, 143902 (2002).

[26] Ullah, K., Jing, H., and Saif, F. , Phys. Rev. A, **97**, 033812 (2018).

[27] Akram, M. J., Ghafoor, F., and Saif, F. ,Journal of Physics B: Atomic, Molecular and Optical Physics, **48**, 065502 (2015).

[28] Schliesser, A., Rivière, R., Anetsberger, G., Arcizet, O., and Kippenberg, T. J. ,Nature Physics, **4**, 415 (2008).

[29] Shahandeh, F., and Ringbauer, M., Quantum, **3**, 125 (2019).

[30] Phillips, William D. ,Rev. Mod. Phys. **70**, 721, (1998).

[31] Bouyer, Philippe, Vincent Boyer, S. G. Murdoch, Guillaume Delannoy, Yann Le Coq, Alain Aspect, and Michel Lécrivain. "RF-induced evaporative cooling and BEC in a high magnetic field." In Bose-Einstein Condensates and Atom Lasers, pp. 165-186. Springer, Boston, MA, (2002).

[32] Smirne, Giuseppe. "Experiments with Bose-Einstein condensates in optical traps." PhD diss., University of Oxford, 2005.

[33] Ball, Philip. "Cool atoms make physics prize matter." (2001): 554-554.

[34] Deissler, Benjamin. "A magnetic trap for evaporative cooling of Rb atoms." PhD diss., University of Virginia, 2003.

[35] Herschbach, Norbert, Paul Tol, Andrey Tychkov, Wim Hogervorst, and Wim Vassen. "Magnetic trapping and evaporative cooling of metastable triplet helium." Journal of Optics B: Quantum and Semiclassical Optics 5, no. 2 (2003): S65.

[36] Ketterle, Wolfgang, "Nobel lecture: When atoms behave as waves: Bose-Einstein condensation and the atom laser". Reviews of Modern Physics **74**, (2002).

[37] Whitfield, John. "Molecules form new state of matter." (2003).

[38] Neuman, K. C., and Block, S. M. (2004). Optical trapping. Review of scientific instruments, 75(9), 2787-2809.

[39] Marangos, J. P. (1998). Electromagnetically induced transparency. Journal of Modern Optics, 45(3), 471-503.

[40] Marangos, J. P., and T. Halfmann. "Electromagnetically Induced Transparency." In Handbook of Optics by Optical Society of America, pp. 23-1. McGraw-Hill, 2001.

[41] Dutton, Zachary. Ultra-slow, stopped, and compressed light in Bose-Einstein condensates. Harvard University, 2002.

[42] Slowe, C., Ginsberg, N. S., Ristroph, T., Goodsell, A., and Hau, L. V. (2005). Ultraslow light and Bose-Einstein condensates: Two-way control with

coherent light and atom fields. Optics and photonics news, 16(5), 30-34.

[43] Safavi-Naeini, Amir H., TP Mayer Alegre, Jasper Chan, Matt Eichenfield, Martin Winger, Qiang Lin, Jeff T. Hill, Darrick E. Chang, and Oskar Painter. "Electromagnetically induced transparency and slow light with optomechanics." Nature 472, no. 7341 (2011): 69.

[44] Kühner, T. D., White, S. R., and Monien, H. (2000). One-dimensional Bose-Hubbard model with nearest-neighbor interaction. Physical Review B, 61(18), 12474.

[45] Lafuente, L., and Cuesta, J. A. (2003). Density functional theory for nearest-neighbor exclusion lattice gases in two and three dimensions. Physical Review E, 68(6), 066120.

[46] O. Morsch and M. Oberthaler, Rev. Mod. Phys. **78**, 179 (2006). I. B. Mekhov, and H. Ritsch, J. Phys. B: At. Mol. Opt. Phys. **45**, 102001 (2012).

[47] A. B. Bhattacherjee, Phys. Rev. A **80**, 043607 (2009). A. Bhattacherjee, Opt. Commun. **281**, 3004 (2008).

[48] M. J. Akram, M. M. Khan, and F. Saif, Phys. Rev. A **92**, 023846 (2015).

[49] R. W. Boyd, Nonlinear Optics, Academic Press, New York, (2010).

[50] He, Qing, Fazal Badshah, Rafi Ud Din, Haiyang Zhang, Yong Hu, and Guo-Qin Ge. "Optomechanically induced transparency and the long-lived slow light in a nonlinear system." JOSA B 35, no. 7 (2018): 1649-1657.

[51] A. H. Safavi-Naeini, T. P. Alegre, J. Chan, M. Eicheneld, M. Winger, Q. Lin, J. T. Hill, D. E. Chang, and O. Painter, Nature (London), **472**, 69 (2011).

[52] Huepe, C., Metens, S., Dewel, G., Borckmans, P., and Brachet, M. E. (1999). Decay rates in attractive Bose-Einstein condensates. Physical review letters, 82(8), 1616.

[53] Söding, J., Guéry-Odelin, D., Desbiolles, P., Chevy, F., Inamori, H., and Dalibard, J. (1999). Three-body decay of a rubidium Bose–Einstein conden-

sate. Applied physics B, 69(4), 257-261.

[54] Jiang, Cheng, Hongxiang Liu, Yuanshun Cui, Xiaowei Li, Guibin Chen, and Bin Chen. "Electromagnetically induced transparency and slow light in two-mode optomechanics." Optics express 21, no. 10 (2013): 12165-12173.

[55] Cromie, William J. (1999-02-18). "Physicists Slow Speed of Light". The Harvard University Gazette. Retrieved 2008-01-26.

[56] Jia, W. Z., Wei, L. F., Li, Y., and Liu, Y. X. (2015). Phase-dependent optical response properties in an optomechanical system by coherently driving the mechanical resonator. Physical Review A, 91(4), 043843.

[57] Huang, Zhilei, Kaiyu Cui, Guoren Bai, Xue Feng, Fang Liu, Wei Zhang, and Yidong Huang. "High-mechanical-frequency characteristics of optomechanical crystal cavity with coupling waveguide." Scientific reports 6 (2016): 34160.

[58] Liu, Chien; Dutton, Zachary; Behroozi, Cyrus H.; Hau, Lene Vestergaard (2001). "Observation of coherent optical information storage in an atomic medium using halted light pulses". Nature. 409 (6819): 490–493.

[59] Pollitt, Michael (2008-02-07). "Light touch could boost fibre optic networks". The Guardian. Retrieved 2008-04-04.

[60] Murugkar, Sangeeta, Israel De Leon, Zhimin Shi, Gisela Lopez-Galmiche, Jeff Salvail, Edwin Ma, Boshen Gao, Andreas C. Liapis, Joseph E. Vornehm, and Robert W. Boyd. "Development of a slow-light spectrometer on a chip." In Integrated Optics: Devices, Materials, and Technologies XVI, vol. 8264, p. 82640T. International Society for Optics and Photonics, 2012.

[61] Yasi, Joseph A. "Quantum Information Storage with Slow and Stopped Light."

[62] P. W. Milonni, Fast light, slow light and lefthanded light (Institute of Physics Publishing, Bristol, 2005).

[63] B. D. Clader and J. H. Eberly, J. Opt. Soc. Am. B. **24**, 916 (2007).

[64] Akram, M. Javed, M. Miskeen Khan, and Farhan Saif. "Tunable fast and slow light in a hybrid optomechanical system." Physical Review A 92, no. 2 (2015): 023846.

[65] Sackett, C. A., and R. G. Hulet. "Dynamics of Bose-Einstein condensation in a gas with attractive interactions." Journal of Optics B: Quantum and Semiclassical Optics 3, no. 3 (2001): R1.

[66] Frese, Daniel. "Bose-Einstein Condensation of Rubidium: Towards Ultracold Binary Bosonic Mixtures." PhD diss., Dissertation, Mathematisch-Naturwissenschaftlichen Fakultät der Rheinischen Friedrich-Wilhelms-Universität Bonn, 2005.